Bi-allelic *PRMT9* loss-of-function variants cause a syndromic form of intellectual disability

Graphical abstract

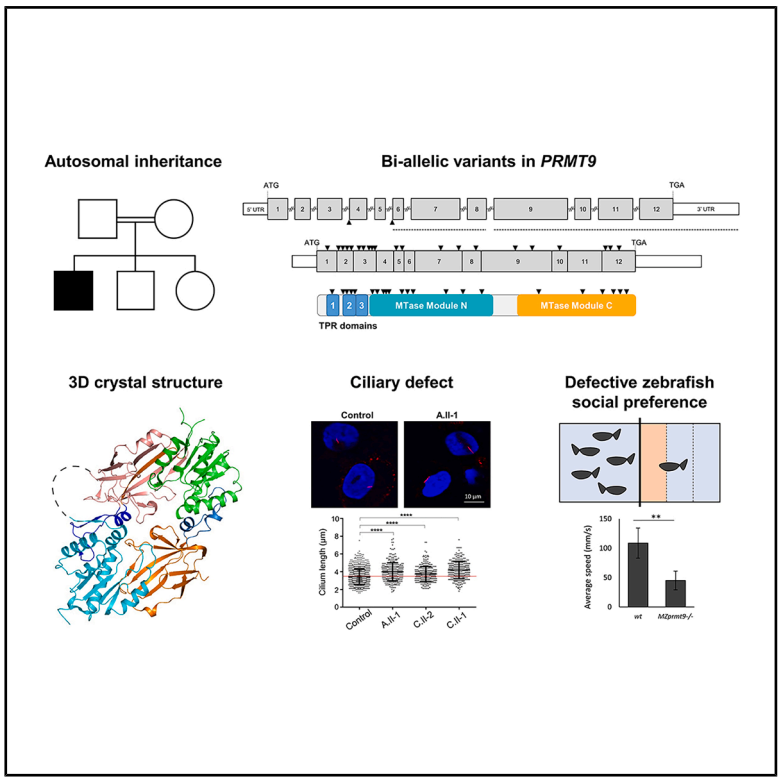

Authors

Ariane Kröll-Hermi, Corinne Stoetzel, Christelle Etard, ..., Uwe Strähle, Hélène Dollfus, Jean Muller

Correspondence

dollfus@unistra.fr (H.D.), jeanmuller@unistra.fr (J.M.)

Bi-allelic loss-of-function variants in protein arginine methyltransferase 9 (*PRMT9*) cause a neurodevelopmental disorder with variable severity. Affected individuals have mild to severe intellectual disability, global developmental delay, autism spectrum disorder, epilepsy, and hypotonia. Functional studies on patients' cells reveal a possible functional impact on ciliary functions.

Kröll-Hermi et al., 2025, The American Journal of Human Genetics *112*, 2943–2960
December 4, 2025

https://doi.org/10.1016/j.ajhg.2025.10.014

Bi-allelic *PRMT9* loss-of-function variants cause a syndromic form of intellectual disability

Ariane Kröll-Hermi,[1,2,63] Corinne Stoetzel,[1,63] Christelle Etard,[2,63] Levon Halabelian,[3,4,5,63] Elise Schaefer,[1,6] Sophie Scheidecker,[1,7] Kimia Kahrizi,[8] Jamali Payman,[8] Véronique Geoffroy,[1,59] Megana Prasad,[1] Cathy Obringer,[1] Laurie Ruch,[1] Amandine Girard,[1] Hong Zeng,[3] Fengling Li,[3] Damien Plassard,[9,10] Céline Keime,[9,10] Francesca Mattioli,[9] Claire Feger,[7] Amélie Piton,[7,9] Atsushi Fujita,[11] Naomichi Matsumoto,[11] Matheus Augusto Araujo Castro,[12] Kim Chong Ae,[12] Lyse Ruaud,[13] Jonathan Levy,[14] Blandine Dozières,[15] Anne-Claude Tabet,[15,16] Ingrid M. Wentzensen,[17] Teresa Santiago-Sim,[17,61,62] Roman Yusupov,[18] Kristian Tveten,[19] Marie Falkenberg Smeland,[19,60] Ebba Alkhunaizi,[20] Gina Cowing,[21] Chumei Li,[21] Saskia B. Wortmann,[22,23] René G. Feichtinger,[22] Johannes A. Mayr,[22] Herman Gonorazky,[24] Gan Jing,[25] Xiaodong Wang,[26] Jia Wang,[26] Tatjana Bierhals,[27] Lev Grinstein,[28] Theresia Herget,[27] Anna Ruiz,[29] Elisabeth Gabau,[30] Antje Kampmeier,[31] Olivier Kassel,[2] Alma Kuechler,[31] Konrad Platzer,[32] Rami Abou Jamra,[32] Audrey Woerner,[33] Michaela Idleburg,[33] Susanne Gerit Kircher,[34]

(Author list continued on next page)

Summary

Protein arginine methyltransferase 9 (PRMT9) is part of the PRMT family, and it is suspected to function in pathways relevant to neurodevelopment. It is thought to participate in alternative splicing through interactions with the splicing factor SF3B2 (SAP145). In this study, we report 26 families (35 individuals) with bi-allelic loss-of-function variants in *PRMT9*, implicating *PRMT9* in an autosomal-recessive human disease. Individuals primarily present with a neurodevelopmental disorder characterized by global developmental delay, learning disabilities, mild to severe intellectual disability, autism spectrum disorder, epilepsy, and hypotonia. The mutation spectrum includes 26 different variants such as frameshifting indels, nonsense variants, missense variants, and two copy-number variants. Mapping of the disease-causing missense variants onto the crystal structure of PRMT9 revealed that several of the variants reside within the catalytically active module of PRMT9, likely impairing its methyltransferase activity and resulting in a loss of function. In skin fibroblasts derived from affected individuals, we observed reduced expression at the RNA and/or protein level and subsequent aberrant methylation activity. Moreover, transcriptomic analysis of fibroblasts from affected individuals indicated differential expression of genes related to intellectual disability, autism, and cilia, suggesting a role of PRMT9 during ciliogenesis. Under ciliogenesis conditions, the skin-derived fibroblasts exhibited anomalies in the length of primary cilia but normal amounts of cilia. In addition, a *prmt9* knockout zebrafish model displayed abnormal social preference in adult animals. Altogether, our findings implicate bi-allelic *PRMT9* loss-of-function variants as causal for neurodevelopmental disorders.

Introduction

Affecting at least 1% of the population worldwide, intellectual disability is a major healthcare problem.[1,2] Defined as a substantive limitation in intellectual functioning and adaptive behavior with an age of onset before 18 years, it is clinically and genetically highly heterogeneous.[3] Sequencing efforts such as trio whole-exome sequencing

[1]Laboratoire de Génétique Médicale, UMR_S INSERM U1112, Institut de Génétique Médicale d'Alsace (IGMA), Faculté de Médecine, Université de Strasbourg, Strasbourg, France;[2]Karlsruhe Institute of Technology (KIT), Institute of Biological and Chemical System (IBCS), Eggenstein-Leopoldshafen, Germany;[3]Structural Genomics Consortium, University of Toronto, Toronto, ON M5G 1L7, Canada;[4]Department of Pharmacology and Toxicology, University of Toronto, Toronto, ON, Canada;[5]Princess Margaret Cancer Centre, University Health Network, Toronto, ON, Canada;[6]Service de Génétique Médicale, Institut de Génétique Médicale d'Alsace, Hôpitaux Universitaires de Strasbourg, Strasbourg, France;[7]Laboratoires de Diagnostic Génétique, Hôpitaux Universitaires de Strasbourg, Strasbourg, France;[8]Genetics Research Center, University of Social Welfare and Rehabilitation Sciences, Tehran, Iran;[9]Institut de Génétique et de Biologie Moléculaire et Cellulaire, INSERM U1258, CNRS UMR 7104, Université de Strasbourg, Illkirch, France;[10]Plateforme GenomEast, Infrastructure France Génomique, Strasbourg, France;[11]Department of Human Genetics, Yokohama City University Graduate School of Medicine, Yokohama, Japan;[12]Unidade de Genetica, Instituto da Crianca, HC FMUSP, Faculdade de Medicina, Universidade de Sao Paulo, Sao Paulo, Sao Paulo, Brazil;[13]Université de Paris, UMR 1141 NEURODIDEROT, INSERM, Département de Génétique, Hôpital Universitaire Robert Debré, APHP Nord, Paris, France;[14]Genetics Department, AP-HP, Robert-Debré University Hospital, Paris, France;[15]AP-HP, Hôpital Robert Debré, Service de Neurologie Pédiatrique et des Maladies Métaboliques, Paris, France;[16]Neuroscience Department, Génétique Humaine et Fonction Cognitive Unit, Pasteur Institute, Paris, France;[17]GeneDx Inc., Gaithersburg, MD 20877, USA;[18]Division of Genetics, Joe DiMaggio Children's Hospital, Hollywood, FL, USA;[19]Department of Medical Genetics, Telemark Hospital Trust, Skien, Norway;[20]Division of Clinical and Metabolic Genetics, Department of Pediatrics, The Hospital for Sick Children, University of Toronto, Toronto, ON, Canada;[21]McMaster University Medical Center, Hamilton, ON, Canada;[22]University Children's Hospital, Paracelsus Medical University (PMU), Salzburg, Austria;[23]Radboud Center for Mitochondrial Medicine, Department of Pediatrics, Amalia Children's

(Affiliations continued on next page)

Franco Laccone,[34] Barbara Golob,[35] Borut Peterlin,[35] Goran Čuturilo,[36,37] Velibor Tasic,[38] Caroline M. Kolvenbach,[39] Friedhelm Hildebrandt,[39] Luiza L.P. Ramos,[40,41] Fernando Kok,[40,41] Cecilia Barbosa Buck,[42] Ingrid M.B.H. van de Laar,[43] Stella A. de Man,[44] Elifcan Taşdelen,[45] Abdullah Sezer,[45] Afife Büke,[45] Zehra Yavuz,[46] Selim Selçuk Çomoğlu,[46] Carrie Costin,[47] Frédéric Tran Mau Them,[48,49] Elodie Lacaze,[50] Thomas Courtin,[51] Delphine Héron,[51] Boris Keren,[51] Sandra Whalen,[51] Joelle Roume,[52] Yanzhong Yang,[53] Mariëtte J.V. Hoffer,[54] Arie van Haeringen,[54] Hossein Najmabadi,[8] Cheryl H. Arrowsmith,[3,55] Uwe Strähle,[2,56] Hélène Dollfus,[1,6,57,*] and Jean Muller[1,5,58,*]

(WES) or whole-genome analysis[3,4] have revealed pathogenic variants in many genes (>1,000 genes) with highly variable conditions and inheritance modes (X-linked, autosomal-dominant, or autosomal-recessive).[5] Autosomal-recessive intellectual-disability-associated genes account for a small fraction of affected individuals in outbred populations.[6] However, it is estimated that the number of known genes will continue to rise in the coming years.[3,7]

In silico analysis of intellectual-disability-related genes revealed that among the most enriched biological functions were cellular metabolism and transport, nervous system development, RNA metabolism, and transcription, including specifically the hedgehog pathway and cilia/centrosome functions.[5] Of interest, more than 50 genes have been described with various forms of intellectual disability as related to ciliopathies, defined as dysfunction of the primary cilium or impaired primary cilium biogenesis. The primary cilium is an organelle that extends from the surface of almost all vertebrate cells and plays a critical role in developmental and homeostatic signaling pathways such as the Sonic Hedgehog (Shh) pathway.[8] Individuals with intellectual disability and pathogenic variants in ciliary genes can have additional symptoms including renal dysfunction, retinal degeneration, limb abnormalities such as polydactyly, and many others.[9]

Here, we report a series of 35 individuals (26 families) with bi-allelic variants in *PRMT9* (MIM: 616125) and delineate associated phenotypic features, which include global developmental delay with intellectual disability, autism, epilepsy, hypotonia, and several variable features such as facial dysmorphism, polydactyly, urogenital anomalies, and endocrine disorders. PRMT9 belongs to the family of protein arginine methyltransferases (PRMTs), a family of currently nine proteins whose main function is thought to be the methylation of arginine residues on histones or other proteins.[10] Functionally, it is thought to participate in alternative splicing through its interaction with the splicing factor SAP145 and by modulating small nuclear ribonucleoprotein maturation.[10] We provide molecular and cellular data implicating *PRMT9*

Hospital, Radboud UMC, Nijmegen, the Netherlands;[24]Division of Neurology, The Hospital for Sick Children, Toronto, ON, Canada;[25]Department of Pediatric Neurology, West China Second University Hospital, Sichuan University, Chengdu, China;[26]Cipher Gene Ltd., Beijing, China;[27]Institute of Human Genetics, University Medical Center Hamburg-Eppendorf, Hamburg, Germany;[28]Department of Pediatrics, University Medical Center Hamburg-Eppendorf, Hamburg, Germany;[29]Genetics Laboratory, Center for Genomic Medicine, Parc Taulí Hospital Universitari, Institut d'Investigació i Innovació Parc Taulí (I3PT-CERCA), Universitat Autònoma de Barcelona, Sabadell, Spain;[30]Paediatric Unit, Parc Taulí Hospital Universitari, Institut d'Investigació i Innovació Parc Taulí I3PT, Universitat Autònoma de Barcelona, Sabadell, Spain;[31]Institute of Human Genetics, University Medical Center Essen, University of Duisburg-Essen, Essen, Germany;[32]Institute of Human Genetics, University of Leipzig Medical Center, Leipzig, Germany;[33]Division of Genetic and Genomic Medicine, Department of Pediatrics, UPMC Children's Hospital of Pittsburgh, Pittsburgh, PA, USA;[34]Institute of Medical Genetics, Center of Pathobiochemistry and Genetics, Medical University of Vienna, Vienna, Austria;[35]Clinical Institute for Genomic Medicine, University Medical Center Ljubljana, Ljubljana, Slovenia;[36]University Children's Hospital Belgrade, Belgrade, Serbia;[37]Faculty of Medicine, University of Belgrade, Belgrade, Serbia;[38]University Children's Hospital, Medical Faculty of Skopje, Skopje, Macedonia;[39]Division of Nephrology, Department of Medicine, Boston Children's Hospital, Harvard Medical School, Boston, MA 02115, USA;[40]Neurogenetics Unit, Department of Neurology, University of Sao Paulo, Sao Paulo 01308-000, Brazil;[41]Mendelics Genomic Analysis, Sao Paulo, Sao Paulo 04013-000, Brazil;[42]School of Medicine, Anhembi Morumbi University, Piracicaba, Sao Paulo 13425-380, Brazil;[43]Department of Clinical Genetics, Erasmus University Medical Center, Rotterdam, the Netherlands;[44]Department of Pediatrics, Amphia Hospital, Breda, the Netherlands;[45]Department of Medical Genetics, Ankara Etlik City Hospital, Ankara, Türkiye;[46]Department of Neurology, Ankara Etlik City Hospital, Ankara, Türkiye;[47]Genetic Center, Akron Children's Hospital, Akron, OH, USA;[48]Unité Fonctionnelle Innovation en Diagnostic Génomique des maladies rares, CHU Dijon Bourgogne, Dijon, France;[49]INSERM UMR1231 GAD, 21000 Dijon, France;[50]Department of Medical Genetics, Le Havre Hospital, Le Havre, France;[51]AP-HP, Département de Génétique, Centre de Référence Maladies Rares "Anomalies du développement et syndromes malformatifs", Hôpital de la Pitié Salpêtrière, Paris, France;[52]Department of Clinical Genetics, Centre de Référence "AnDDI Rares", Poissy Hospital GHU PIFO, Poissy, France;[53]Department of Cancer Genetics and Epigenetics, Beckman Research Institute, City of Hope Cancer Center, Duarte, CA, USA;[54]Department of Clinical Genetics, Leiden University Medical Center, Leiden, the Netherlands;[55]Princess Margaret Cancer Centre and Department of Medical Biophysics, University of Toronto, Toronto, ON M5G 2M9, Canada;[56]Centre for Organismal Studies (COS), University of Heidelberg, Im Neuenheimer Feld 223, 69120 Heidelberg, Germany;[57]Centre de Référence pour les affections rares en génétique ophtalmologique (CARGO), Filière SENSGENE, Hôpitaux Universitaires de Strasbourg, Strasbourg, France;[58]Unité Fonctionnelle de Bioinformatique Médicale appliquée au diagnostic (UF7363), Hôpitaux Universitaires de Strasbourg, Strasbourg, France
[59]Present address: INSERM, Univ Brest, EFS, CHU Brest, UMR 1078, GGB (Génétique, Génomique fonctionnelle et Biotechnologies), Faculté de Médecine, Brest, France
[60]Present address: Department of Pediatric Rehabilitation, University Hospital of North Norway, 9038 Tromsø, Norway
[61]Present address: Department of Molecular and Human Genetics, Baylor College of Medicine, Houston, TX 77030, USA
[62]Present address: Baylor Genetics Laboratories, Houston, TX 77021, USA
[63]These authors contributed equally
*Correspondence: dollfus@unistra.fr (H.D.), jeanmuller@unistra.fr (J.M.)
https://doi.org/10.1016/j.ajhg.2025.10.014.

loss of function (LoF) in an autosomal-recessive form of intellectual disability. Furthermore, we provide insight into the pathophysiological mechanisms linking cilia dysfunction to a neurodevelopmental condition.

Subjects and methods

Subjects

Following written consent from each participant and/or their parents, whole blood, DNA, or skin fibroblasts were obtained from each research participant. Study protocols used in our cohort have been approved by the corresponding Institutional Review Board or equivalent local committees (see supplemental information). Our research was conducted in concordance with the Declaration of Helsinki. Written informed consent of all examined individuals or their legal representatives for genetic testing and the publication of findings was obtained after advice and information about the risks and benefits of the study.

Pathogenic variant identification

This study involves 25 unrelated families from different institutions worldwide. All research participants except family B (already reported in Najmabadi et al.[7]) were contacted by way of DECIPHER[11] or GeneMatcher.[12] They were all investigated using whole-exome sequencing, and variants were confirmed using either CGH/SNP array and/or Sanger sequencing (see supplemental methods).

Cell culture

Primary skin fibroblasts of the affected individuals (A.II-1, C.II-1, and C.II-2) and healthy control individuals of the same age and sex were obtained from skin biopsies as previously described.[13] Fibroblasts were cultivated at 37°C and 5% CO_2 in DMEM + GlutaMAX (ref. 21885-025, Thermo Fisher Scientific, USA) supplemented with 10% fetal calf serum (FCS) and 1% penicillin-streptomycin-glutamine (PSG). To induce primary cilium formation, the cells were deprived of serum by growth for 48 h in DMEM with 1% PSG.

Real-time quantitative PCR

Total RNA from fibroblasts derived from affected individuals was extracted with the RNeasy kit (#74104, Qiagen, Germany). RNA integrity was evaluated by agarose gel electrophoresis, and RNA concentration was determined with the Qubit RNA assay kit (ref. Q32852, Thermo Fisher Scientific) according to the manufacturer's instructions. Reverse transcription of 1 μg total RNA to complementary DNA (cDNA) was performed using the Bio-Rad iScript cDNA Synthesis Kit (#170-8891, Bio-Rad, USA), which uses a blend of oligo(dT) and random hexamer primers, according to the manufacturer's instructions. Real-time quantitative PCR (qPCR) amplification was performed in a Bio-Rad CFX96 Real-Time System using the iQTM SYBR Green SuperMix (#170-8886, Bio-Rad) and primer sets (Table S3) with optimized conditions (efficacy and melt curves). Reactions were set up in triplicate and, depending on the experiment, either one or three controls were used. Gene-expression levels were quantified relative to the reference genes *GAPDH* and *ACTB* (β-actin) using the efficiency-corrected comparative cycle threshold (C_T) method and the CFX Manager Software v.1.5 (Bio-Rad).

Immunofluorescence

Primary cells were grown in Nunc Lab-Tek Chamber Slides (Thermo Fisher Scientific), and ciliogenesis was done as described in the cell culture section. Primary cilia were labeled with an antibody directed against acetylated α-tubulin (red), and nuclei were stained with 1:2,000 Hoechst 33258 pentahydrate (Life Technologies, blue). The slides were mounted with Vectashield (Vector Laboratories). Cells were imaged by a fluorescence microscope (Zeiss Axio Observer D1). The length of primary cilia was measured on the pictures using ImageJ. Primary and secondary antibodies used in this study, as well as their dilution, are presented in Table S4.

Western blotting

Total protein from three controls and affected individuals' fibroblasts (A.II-1 and C.II-2) were extracted with non-denaturing lysis buffer (20 mM Tris-HCl [pH 8], 137 mM NaCl, 10% glycerol, 1% Nonidet P-40 [NP-40], 2 mM EDTA, and 1× Cocktail Roche [protease inhibitor cocktail]) and separated in SDS-Laemmli gels (10%). Separated proteins were transferred onto a polyvinylidene difluoride (PVDF) membrane blocked for 2 h in 5% milk in Tris-buffered saline and Tween 20 (Sigma-Aldrich, #P1379-500ML) (TBST), then incubated overnight under agitation at 4°C with the relevant primary antibody (PRMT9, SAP145, SDMA, and β-tubulin). After incubation, membranes were washed six times with TBST and incubated with an appropriate secondary antibody conjugated to horseradish peroxidase. Finally, proteins were detected with the SuperSignal West Femto Maximum Sensitivity Substrate (Thermo Fisher Scientific, #34095) or the Pierce ECL Western Blotting Substrate (Thermo Fisher Scientific, #32209) according to the instructions in the kit's manuals using the Molecular Imager Gel Doc XR System (Bio-Rad). The molecular weight of the bands was estimated using the Precision Plus Protein WesternC Standard (Bio-Rad, #161-0376). A list of antibodies used in this study is available in Table S4.

PRMT9 production, purification, crystallization, and structural determination

Human PRMT9 (127–845 amino acids [aa]) was subcloned into a vector encoding an N-terminal His_6 tag, followed by a tobacco etch virus (TEV) cleavage site, and expressed in *sf9* cells.[14] The recombinant PRMT9 protein was first affinity purified with Talon beads, followed by size-exclusion chromatography using an S200 column pre-equilibrated with 20 mM Tris-HCl (pH 8.0) and 150 mM NaCl. The N-terminal His_6 tag was then cleaved by incubating the protein with TEV protease at 4°C overnight. The protein was further purified to homogeneity using an ion-exchange Source Q column pre-equilibrated with 20 mM Tris-HCl (pH 7.5) (buffer A) and eluted with 20 mM Tris-HCl (pH 7.5) and concentration gradient of 1 M NaCl (buffer B). The measured mass after TEV cleavage was 80,406.19 Da, as determined by mass spectrometry. Apo-PRMT9 diffraction-quality crystals were obtained in vapor-diffusion sitting drops by mixing equal volumes of PRMT9 at 8.8 mg/mL and precipitant solution containing 20% (w/v) polyethylene glycol 3350 and 0.2 M ammonium nitrate. Crystals were then cryo-protected using reservoir solution supplemented with 10% (v/v) ethylene glycol and cryo-cooled in liquid nitrogen. X-ray diffraction data for Apo-PRMT9 were collected at the 24ID-E beamline at the Advanced Photon Source. Data were processed with XDS.[15] Initial phases were obtained by MR-Rosetta.[16] Model building was performed in COOT[17] and

refined with Buster.[18] MolProbity[19] was used for structural validation. Images were prepared in PyMOL.[20] Data collection and refinement statistics for Apo-PRMT9 are summarized in Table S5.

The six truncated PRMT9 missense variants (127–845 aa)—PRMT9-E7 (c.773A>T [p.Asp258Val]), PRMT9-E8 (c.1772T>C [p.Phe591Ser]), PRMT9-E9 (c.1144C>A [p.Gln382Lys]), PRMT9-E10 (c.2405C>T [p.Thr802Ile]), PRMT9-E11 (c.554G>A [p.Gly185Glu]), and PRMT9-E12 (c.565G>A [p.Gly189Arg])—were subcloned into the pFBOH-MHL vector (Addgene #62304). The resulting constructs were expressed and purified similar to the wild-type PRMT9 described above.

Differential scanning fluorimetry

Wild-type PRMT9 and its missense variants were each diluted to 0.1 mg/mL in a buffer containing 100 mM HEPES (pH 7.5), 150 mM NaCl, and 5× SYPRO Orange dye (Life Technologies, S-6650). A volume of 20 μL was dispensed per well into a white polypropylene 384-well plate (Axygen, #UC500). Differential scanning fluorimetry (DSF) was performed using a LightCycler 480 II system (Roche Applied Science, Penzberg, Germany) with a temperature ramp of 4°C/min from 20°C to 95°C. Fluorescence readings were collected at 0.5°C intervals. Melting temperatures (T_m) were determined by fitting the fluorescence data to a Boltzmann sigmoid curve.

Transcriptome analysis: RNA sequencing

RNA samples were extracted from fibroblasts of individual A.II-1, C.II-1, C.II-2, and three controls in two conditions using ciliary and non-ciliary conditions for cell culture[21] (see cell culture section) using TRI reagent (Molecular Research Center) or the RNeasy Mini Kit (Qiagen). Both protocols included an additional step of recombinant DNase I treatment (Sigma-Aldrich). The integrity and quality of the RNA were evaluated on a 1% bleach agarose gel by electrophoresis[22] on an RNA 6000 Nano Chip on the bioanalyzer (Agilent Technologies). Library preparation was performed at the GenomEast platform at the Institute of Genetics and Molecular and Cellular Biology (Strasbourg, France) using the TruSeq RNA sample preparation v.2 protocol (Illumina) starting from 1 μg of extracted total RNA. Libraries were then 2 × 100-bp paired-end sequenced on an Illumina Hiseq4000 sequencer generating between 92 and 162 million paired reads per sample. The corresponding bioinformatics pipeline is described in detail in the supplemental information.

Generation of MZ*prmt9*$^{-/-}$ zebrafish models

The wild-type zebrafish AB_2O_2 strain was obtained from the European Zebrafish Resource Center (EZRC, Karlsruhe). *prmt9*^{ka709} mutant alleles were generated using the CRISPR-Cas9 system. The CRISPR guide RNA was designed with ChopChop software (binding sequence: CCTTCACCGGAAATCTCTGGACA) and synthesized with the MEGAshortscript T7 Transcription Kit (Ambion) according to the manufacturer's instructions. *prmt9* guide RNA and Cas9 protein (GeneArt Platinum Cas9 Nuclease, Invitrogen) were co-injected into one-cell-stage embryos (300 ng/μL each), and animals were raised until adulthood. F0 mosaic founders were outcrossed with wild-type fish. The resulting F1 adults were fin clipped as previously described.[23] Genomic DNA was HotSHOT extracted with 100 μL of 50 mM NaOH and 10 μL Tris-HCl (pH 7.5) and then neutralized. A PCR covering the guide RNA binding sequence was performed followed by Sanger sequencing (Microsynth). Primers are listed in Table S3. F1 heterozygous fish with a 4-bp insertion were identified and incrossed to obtain homozygous zygotic *prmt9* mutants (Z*prmt9*^{ka709}). To obtain maternal zygotic mutants (MZprmt9^{ka709}), Z*prmt9*^{ka709} mutant adults were incrossed. For real-time qPCR, total RNA from 50 embryos was extracted using TRIzol reagent (Invitrogen) following the manufacturer's protocol, reverse transcribed with the Maxima First Strand cDNA Synthesis Kit (Thermo Fisher Scientific), and amplified with GoTaq 1-Step-RT-qPCR System (Promega) using the StepOnePlus Real-Time PCR System (Thermo Fisher Scientific). Wild-type zebrafish and *prmt9*^{ka709} mutants were raised as described previously,[24] and experimental procedures were performed in accordance with German animal protection regulations (Regierungspräsidium Karlsruhe, Germany, AZ35-9185.81/G-184-17). Embryos were raised in 1× Instant Ocean salt solution at 28.5°C (Aquarium Systems) and staged according to Kimmel et al.[25]

Whole-mount *in situ* hybridization: Zebrafish embryos

To suppress melanogenesis, embryos were raised in water supplemented with 0.003% phenylthiourea (PTU). *In situ* hybridization was performed as previously described.[26] Probes targeting *krox20* and *msxc* have been described.[27] To examine the expression of *prmt9* in embryos, a probe binding 552 bp of the *prmt9* transcript was designed and amplified from 3-day post-fertilization wild-type embryo cDNA. The amplicon was cloned into the pGEMT-easy vector (Promega).[28] We used Apa1 to linearize the plasmid and SP6 to transcribe DIG-labeled antisense RNA probes.

Social preference test of adult zebrafish

For the social preference test, we used adult males as described by Liu et al.[29] Standard 1-L breeding tanks divided into two compartments with a clear barrier were used to separate a single fish (mutant or wild type) from a conspecific group of five fish. The behavior of each test individual was assessed only once to avoid repeated stress as well as any possible habituation and repeated six times (biological replicates). After an acclimation period of 5 min, the fish movements were recorded for 10 min and the swimming behavior analyzed with the ToxTrac tool.[30,31]

Statistics

For *in vitro* and *in vivo* experiments, sample sizes were chosen according to the standard practice in the field for each known genotype. For humans, sample size was limited by the samples available. In all zebrafish experiments, samples (n) represent a random selection of a bigger cohort for each genotype considered. The status of the zebrafish (wild type or mutant) was always known to the experimenters. Results are reported as mean ± standard deviation (SD) or standard error of the mean (SEM) for the number of experiments indicated in the legends of each figure or table. Statistical analyses were performed using either Excel (Microsoft, USA) or the Prism software (GraphPad, USA). In most of the instances, we used a Student's t test to compare two groups of normally distributed data. Statistical significance was set according to the levels at $p = 0.05$, and was indicated by $^{*}p < 0.05$, $^{**}p < 0.01$, $^{***}p < 0.001$, and $^{****}p < 0.0001$. Non-normally distributed data were compared using a Wilcoxon (Mann-Whitney) non-parametric test for unpaired data. Significance levels and number of samples/replicates are indicated in each figure legend. All p values for main figures and supplemental figures can be found in Table S14.

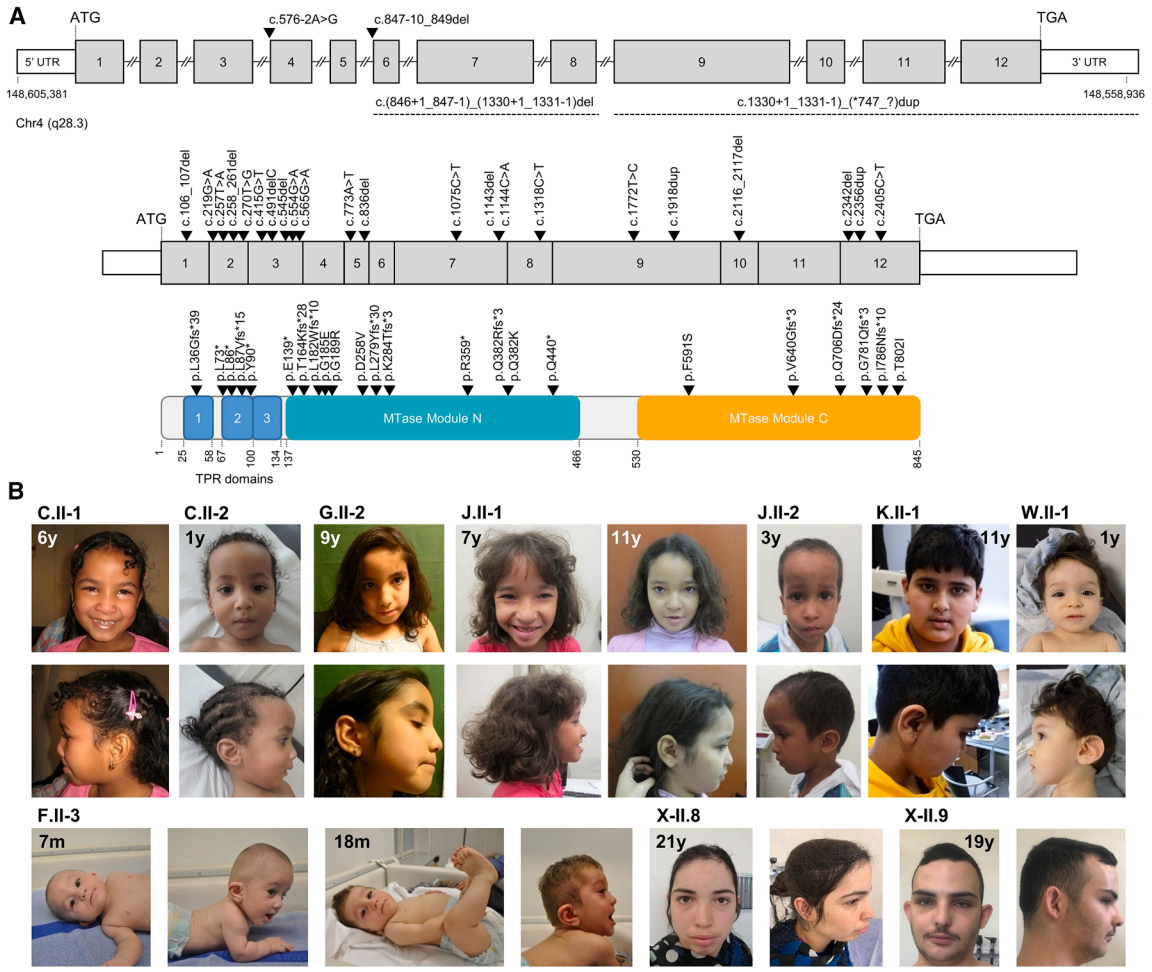

Figure 1. Individuals and variants identified in *PRMT9*

(A) Schematic of the *PRMT9* locus, mRNA, and protein with the different protein domains. Variation positions are given according to the RefSeq identifiers GenBank: NM_138364.3 and NP_612373.2.

(B) Face (upper) and profile (lower) photographs for individuals with bi-allelic pathogenic variant in *PRMT9* for families C, F, G, J, K, W, and X.

Results

Identification of bi-allelic LoF variants in *PRMT9*

The proband (A.II-1) is the first-born child of three sibs from a consanguineous union in a family of Algerian origin (Figure S1). Due to the presence of bilateral post-axial polydactyly, developmental delay, and a suspected and subsequently ruled out retinal dystrophy, a ciliopathy and, more specifically, a Bardet-Biedl syndrome (BBS [MIM: 209900]) was first suspected (Table S1). Other clinical manifestations included poor muscle tone, bilateral cryptorchidism, spontaneously resolving vesicoureteral reflux, and a mildly dysmorphic facial gestalt. His birth size and weight were within the normal range. With time, he demonstrated autistic behavior connected to major anxiety. At the age of 7 years old, he had his first seizure, which has since been pharmacologically controlled. Cerebral magnetic resonance imaging (MRI) revealed the presence of bilateral periventricular nodular heterotopia. At the last clinical examination at age 9, the proband had severe intellectual disability with a near complete lack of language. He had normal weight, height, and head circumference. Ophthalmological examination did not reveal any abnormalities. After screening of known BBS-associated genes and related phenotypes without identifying causal variants (see supplemental information), WES and homozygosity mapping were performed. Following classical filtering strategy including functional criteria, sequence quality, frequency in population-based databases, and overlapping homozygous regions (Figure S2), only a small subset of variants remained (see supplemental methods; Figures S3 and S4). We focused on an inherited homozygous single-nucleotide deletion in exon 3 (c.545delT [GenBank: NM_138364.3 [PRMT9]]) (p.Leu182Trpfs*10) of *PRMT9* (Figures S2 and S5A). *PRMT9* is located on chromosome 4 (4q31.23) encompassing 46.4 kb and 12 exons. The only coding mRNA transcript is ~3.5 kb long and encodes a protein of 845 aa (94.5 kDa) (Figure 1A) with low tissue specificity.[32]

Table 1. Distribution of clinical characteristics within the *PRMT9* cohort ($n = 35$ individuals maximum)

	No. of affected individuals
Neurological	
Intellectual disability, mild to severe	29/30
Cerebral MRI anomalies	12/26
Epilepsy	14 (15)/35
Autistic behavior	8 (10)[a]/29
Hypotonia	17/28
Development	
Global developmental delay	33/34
Delayed speech and language development	30/34
Facial dysmorphism	28/32
Digit anomalies	13/19
Postaxial polydactyly	5/19
Heart defects	6/16
Kidney defects	3/24
Genital anomalies	8/17
Cryptorchidism	5/17
Endocrine anomalies	9/15

The number of individuals exhibiting a given clinical characteristic is compared to the number of individuals for whom this characteristic could be assessed.
[a]Including suspected affected individuals.

Using DECIPHER[11] and GeneMatcher,[12] we were able to recruit 25 additional families (total $n = 26$, families A to Z), of which more than half ($n = 14$) were characterized by consanguinity (Figure S1 and Table S1). Array or sequencing techniques were used to investigate 35 affected family members (from one to three per family) carrying potential LoF variations in *PRMT9* (supplemental methods) and confirm bi-allelic status in 24 families (Figure S2). In total, 35 individuals from 26 families harbored 26 different potential pathogenic variations in *PRMT9* (Figure S1 and Table S7), including one large deletion of exons 6–8, frameshifting indels ($n = 10$), nonsense variants ($n = 7$), missense variants ($n = 6$), and canonical splice site variants ($n = 2$) (Figure 1A). In one family (family Z), a gain of a single copy of at least exons 9–12 *PRMT9* (variant of uncertain significance) was detected, but no second pathogenic allele in the gene could be identified by WES. The list of variants and their occurrence in the cohort together with their pathogenicity evaluation is described in Tables S7 and S8.

Clinical features of individuals with *PRMT9* variants

Comparing the phenotypic characteristics of the 35 affected individuals including 21 males and 14 females (Tables 1 and S1), we noticed a wide spectrum of neurodevelopmental phenotype in all individuals. Most of the individuals present global developmental delay and mild to severe intellectual disability (33 and 29 individuals, respectively). Hypotonia was noticed in 17 individuals. Autism spectrum disorder (ASD) was suspected or diagnosed in ~30% (10/29) of the affected individuals and was suspected in two others. Developmental language delay was present in 30 individuals, with no language in two of them. Moreover, clinical examinations revealed that 14 individuals developed epilepsy, which was suspected in one other individual. Brain MRI was conducted in 26 affected individuals and showed different nonspecific abnormalities in 12 of them (periventricular heterotopia, white matter abnormalities, *megacisterna magna*, and wide pericerebral spaces). Growth delay and short stature were observed in nine individuals with height ranging between −2.0 and −4.7 SD. Moreover, many individuals presented other features including ophthalmological involvement (strabismus, esotropia, and microphthalmia) in seven individuals, urogenital anomalies in eight individuals including five with cryptorchidism (5 of 17 males), and heart defects in five individuals. Endocrine disorders such as diabetes, obesity, hypothyroidism, and puberty delay were diagnosed in nine individuals. In 28 individuals, nonspecific facial features were observed, including flat facial profile, prominent forehead and frontal bossing, thick eyebrows, hypertelorism, and thin lips (Figure 1B). Skin lesions, such as supernumerary nipple, hypertrichosis, and café-au-lait spots, were observed in seven individuals. Digit anomalies were noticed in 13 individuals including five with postaxial polydactyly.

Effect of the homozygous c.545del frameshift variant on *PRMT9* expression

To investigate the effect of the identified *PRMT9* variation in family A (c.545delT [p.Leu182Trpfs*]), we analyzed the mRNA and protein levels in the proband's skin fibroblasts. In three independent experiments, the expression of *PRMT9* mRNA was significantly decreased in the proband's cells by ~60% as compared to control cells (Figure S5B), suggesting an involvement of the nonsense-mediated mRNA decay (NMD) pathway. Moreover, we examined the effect of the premature stop codon at the protein level of PRMT9. Proteins from the proband's fibroblasts and control cells were extracted and analyzed by western blot using an antibody specific to the N-terminal part of PRMT9. However, we observed neither the full-length protein (Figure S5C) nor a truncated form (data not shown) of PRMT9 in the proband's cells, suggesting that the shortened protein is unstable.

Structural insights into Apo-PRMT9 and evaluation of missense variants

PRMT9 belongs to the family of PRMTs, a family of currently nine proteins whose main function is thought to be the methylation of arginine residues on histones or other proteins.[10] As a type II methyltransferase, PRMT9 is able to generate monomethylarginines (MMAs) and symmetric dimethylarginines (SDMAs).

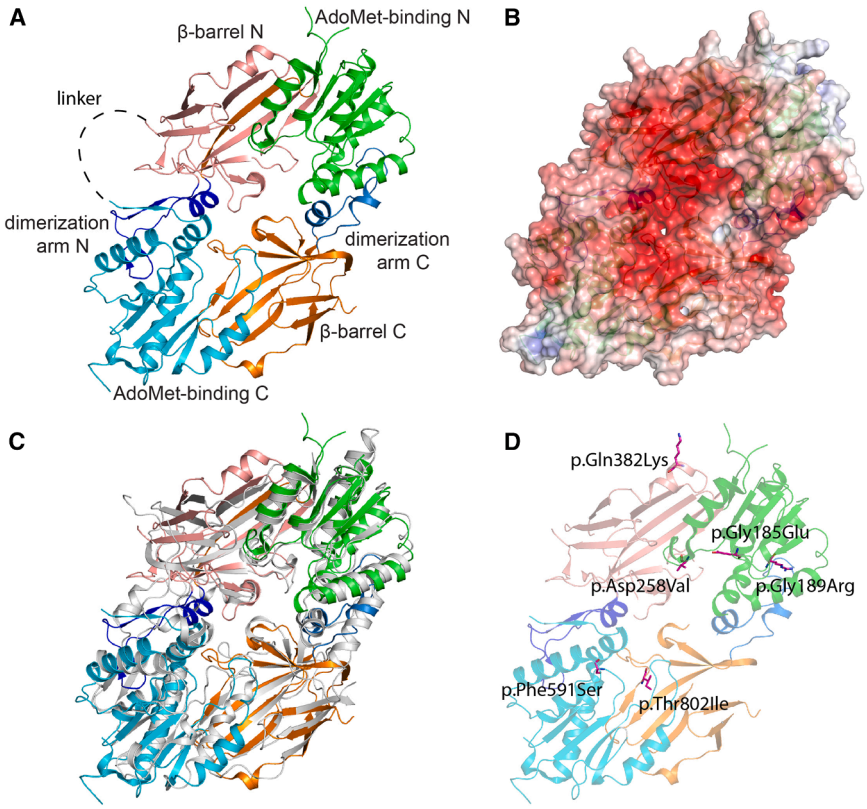

Figure 2. Structural characterization of PRMT9, highlighting the identified missense sites

(A) Crystal structure of the Apo-PRMT9 shown in cartoon representation and color coded according to its domain architecture as labeled. The unresolved linker joining the two modules is displayed as a black dashed line.

(B) Electrostatic surface potential representation of the Apo-PRMT9 shown in the same orientation as in (A). Surface color indicates electrostatic potential ranging from −10 kT/e (red) to +10 kT/e (blue). Electrostatic surface potentials were calculated using APBS.[36]

(C) Overlay of the Apo-PRMT9 monomer, color coded the same as in (A), on *Mm*PRMT7 (gray) (PDB: 4C4A).

(D) Overview of all six missense variants, shown as sticks and colored magenta, distributed among Apo-PRMT9 monomer and color coded the same as in (A).

PRMT9 contains three N-terminal tetratricopeptide repeats (TPRs), which is unique among the human PRMTs, followed by two tandem methyltransferase (MTase) modules—a catalytically active MTase module (called module N) and an inactive MTase module (called module C)—as a result of ancestral gene-duplication events[33] (Figure S6). Interestingly, the two missense variants (p.Gly185Glu and p.Gly189Arg) identified in families B, C, and I are located within two of the three highly conserved glycines in the core motif (motif I) defining the AdoMet binding pocket, one of the critical catalytic sites of PRMTs[34] (Figure S7A). To better understand the functional consequences of PRMT9 pathogenic variants, we determined the crystal structure of the double MTase modules of human PRMT9 in Apo form (referred to here as Apo-PRMT9) (Table S5), which represents the last remaining experimental structure among the nine mammalian PRMT proteins.[34] In the Apo-PRMT9 structure, the two MTase modules are arranged in a head-to-tail pattern forming a bowl-shaped pseudodimer (Figure 2A), similar to the previously observed PRMT7 structure (PDB: 4C4A)[35] (Figure 2C). Each MTase module in PRMT9 contains an N-terminal AdoMet-binding domain (residues 150–297 for module N and 515–692 for module C) and a C-terminal β-barrel domain (residues 298–473 for module N and 694–845 for module C). Additionally, each module contains a dimerization arm (residues 310–338 for module N and 705–734 for module C) inserted within the N-terminal region of each β-barrel domain, which mediates the dimerization interaction between the two modules (Figure 2A). PRMT9 contains a well-defined negatively charged surface at the core region of the bowl for substrate recognition and binding (Figure 2B). Compared to other human PRMTs, PRMT9 is structurally most similar to PRMT7 (Figure 2C). The catalytically active N module of PRMT9 superposes well with the N module of PRMT7 in complex with *S*-adenosyl-homocysteine (AdoHcy, SAH) (PDB: 4C4A), with root-mean-square deviation of 1.42 Å over 244 aligned Cα atoms. However, the zinc-binding motif that is located between the N and C modules of PRMT7 is not conserved in PRMT9[35]; the linker between MTase modules in PRMT9 (residues 474–514) is not resolved in our structure and is likely disordered. Comparison of the catalytically active module N of PRMT9 with the other human PRMTs can be found in Table S6.

Previous analyses by Yang et al. showed that mutating the motif I region in module N of PRMT9 is sufficient to inhibit its methyltransferase activity,[33] suggesting that module C of PRMT9 is catalytically inactive. Our structure of Apo-PRMT9 provides insight into why the MTase module C is inactive and the likely consequence of individuals' variations (Figure 2D). The AdoMet-binding C of PRMT9 is unable to bind AdoMet: substitution of conserved glycines (highlighted in bold) in motif I (VLD/V**G**xGx**G**) into Ser588 and Ser592, distorts the motif I loop conformation such that it occludes cofactor binding (Figure S7B). Similarly, two of the missense variants described in our study (p.Gly185Glu and p.Gly189Arg) substitute the conserved glycines (highlighted in bold) in motif I (VLD/V**G**xGx**G**) of the AdoMet-binding N of PRMT9 into Glu185 and Arg189 that may distort motif I loop conformation and prevent AdoMet from binding into module N of PRMT9 and, thereby, inhibit its MTase activity (Figure S6C).

Other missense variants have prediction scores that are in accordance with a possible pathogenic effect (Table S8). Among these, Asp258 is highly conserved within the PRMT9 and PRMT7 subfamilies and absent from the others (Figure S7A). Given its localization in the substrate-binding pocket of the catalytically active module N of PRMT9 (Figure S7E), the p.Asp258Val variant might interfere with the substrate arginine side-chain recognition and binding. The p.Phe591Ser is inserted inside a hydrophobic pocket located on the catalytically inactive AdoMet-binding domain (module C) of PRMT9 (Figure S7B), which is less conserved compared to the AdoMet-binding domain (module C) of MmPRMT7, assuming it contributes to the protein's overall folding and stability. The position is relatively well conserved but appears specific to the PRMT9 subfamily (Figure S7A). Gln382 is not so well conserved within PRMTs, and is located at the surface region of β-barrel N of PRMT9 with less possible effect on the protein function (Figure S7E). However, looking at the position of the variant relative to the exon boundaries (−3 bases in 5′ from the donor splice site) and according to bioinformatics predictions, the variant might have an effect on splicing rather than as a missense (Table S8). Thr802 is highly conserved within the PRMT9 and PRMT7 subfamilies and absent from the others (Figure S7A). The variation, located in β-barrel C of catalytically inactive module C within a hydrophobic pocket, may disrupt the proper folding of this domain, as Ile side chain is bigger than Thr and may not be properly accommodated inside this pocket (Figure S7D).

Upon expressing the six PRMT9 missense variants in *Sf9* insect cells, we were unable to detect the p.Phe591Ser and p.Thr802Ile variants, suggesting a major folding defect consistent with our structural analysis (Figure S8A). To assess the impact of disease-causing variants on PRMT9 protein stability, we performed DSF. Compared to wild-type PRMT9, the p.Gly189Arg variant showed significant destabilization, with a ΔT_m decrease of 7.2°C. In contrast, the p.Asp258Val variant resulted in a mild destabilization (ΔT_m decrease of 1.3°C). The remaining variants exhibited no significant differences in thermal stability compared to wild-type PRMT9 (Figure S8B).

Nonfunctional PRMT9 does not impair ciliogenesis but affects both ciliary length and function

Given the initial suspicion of a ciliopathy phenotype in the proband (A.II-1), we examined whether cilia could be affected in individuals' cells. We compared skin fibroblasts from individuals A.II-1, C.II-1, and C.II-2 vs. controls under two conditions: normal condition (+FCS) and ciliary condition (−FCS). Counting the number of ciliated cells did not show any difference (Figures 3A and 3B). Nevertheless, the primary cilia length showed significantly longer cilia in the individuals' cells compared to controls (Figure 3C).

To further evaluate a possible impact of *PRMT9* variant on primary cilium function, we measured the Shh pathway activity by measuring GLI1 and PTCH1 essential components (as well as target genes) in patients and control cells. Activation of the signaling is achieved using the smoothened agonist (SAG) under two conditions: normal (+FCS) and ciliary (−FCS). Control samples demonstrated, as expected, a robust induction of these target genes under ciliogenesis conditions (Figure 3D, condition +FCS − SAG vs. −FCS + SAG). In contrast, the individual's cells showed a significantly higher response to SMO ligand stimulation, as confirmed by an increased expression of the pathway target genes under the same condition (Figure 3D, condition −FCS + SAG). These results point to a possible effect of the *PRMT9* variants on the ciliary biogenesis or function.

PRMT9 fails to methylate the splicing factor SAP145 in affected skin fibroblasts

PRMT9 interacts with and methylates the splicing factor SAP145.[10] This in turn stimulates the SAP145 interaction with Survival of Motor Neuron (SMN), a protein required for the assembly of small nuclear ribonucleoprotein particles that are essential for pre-mRNA splicing (Figure 4A).[10] To examine the effect of the *PRMT9* LoF variants (c.545delT, c.554G>A [p.Gly185Glu], and c.1318C>T [p.Gln440*]) from families A and C, a western blot was performed to determine whether SAP145, the target of PRMT9, could still be methylated or not. For this we used an antibody specific for symmetrically dimethylated Arg508 of SAP145 (SDMA).[10] While SAP145 was detected in control and individual cells (A.II-1 and C.II-2), SDMA was only detected in the control (at a low level), showing that the *PRMT9* variants identified in family A (absence of PRMT9) and C (nonfunctional PRMT9) prevent the methylation of the splice factor (Figure 4B). In control cells, no significant difference in PRMT9, SAP145, or SDMA expression could be observed in normal and ciliated conditions (Figure S9).

Bi-allelic *PRMT9* variants affect the expression of genes associated with intellectual disability, ASD, and cilia

PRMT9 activity in alternative splicing, through its interaction with the splice factor SAP145,[10] is especially important in neuron development.[37] We examined the RNA differential expression in probands' cells with a specific focus on genes associated with intellectual disability,[3,38] ASD,[39] and cilia function/biogenesis[40] (Tables 2 and S2). RNA sequencing was performed on the same three samples (A.II-1, C.II-1, and C.II-2) under either rich medium conditions (+FCS) or under ciliated conditions (−FCS) (see supplemental methods and Table S9). To detect the effect of *PRMT9* variations, we focused on shared differentially expressed genes (DEGs) of all three affected individuals (see supplemental methods and Table S9). In total, 62 DEGs were found in cells cultured with FCS, of which 26 were upregulated and 36 downregulated (Figure 5A and Table S10). Considering the cells under ciliary conditions (−FCS), 241

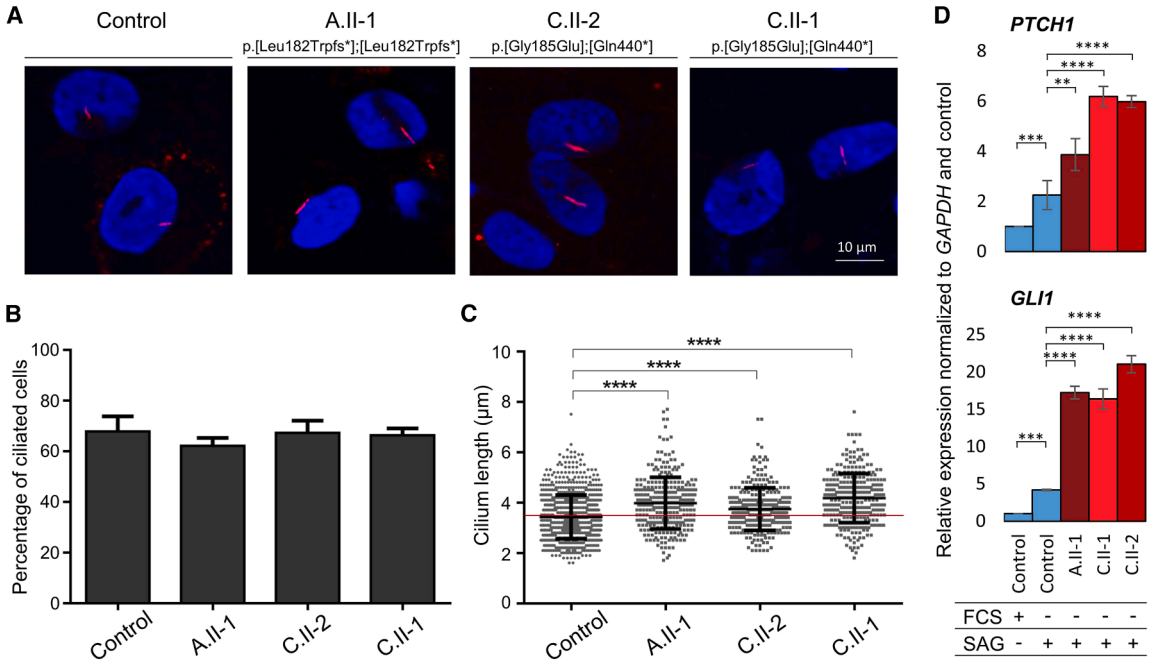

Figure 3. Pathogenic variants in *PRMT9* affect the cilia length of skin fibroblasts from affected individuals

(A) Fibroblasts from control and individuals' cells in ciliary conditions were stained with an antibody against acetylated α-tubulin (cilia, red). Nuclei were stained with DAPI (blue).

(B) Based on 20 fields in three independent experiments (100–150 cells per experiment), mean percentages of ciliated cells of unaltered individual cells compared to control cells are shown in a histogram. The control is the mean of three independent controls, and error bars represent standard deviation.

(C) Individual cells present longer cilia. Data are presented as a scatterplot with a line indicating the mean value and error bars indicating the standard deviation. The control is the mean of three independent controls. Statistical significance was determined using the unpaired non-parametric Mann-Whitney test ($n = 300$; ns, not significant; *$p < 0.05$, **$p < 0.01$, ***$p < 0.001$, ****$p < 0.0001$).

(D) Assessment of Hh-signal transduction by quantification of the expression levels of two Hh target genes (*PTCH1* and *GLI1*) on Hh-stimulated cells (+SAG) from controls and the individual with (−FCS) and without (+FCS) inducing ciliogenesis. All the results are representative of three different experiments. Data are presented as relative expression levels ± SEM. *p* values were calculated using a two-way ANOVA test (Tukey's multiple comparison test). ns, not significant; **$p < 0.01$, ***$p < 0.001$, ****$p < 0.0001$.

DEGs could be identified, of which 75 were upregulated and 166 downregulated (Figure 5A and Table S12).

Among the significant DEGs identified in rich conditions (+FCS), two genes, *SHROOM4* and *SATB2*, are known to be associated with intellectual disability and eight genes, *PCDH10*, *HCLS1*, *PLXDC2*, *RTN1*, *TIPARP*, *CD44*, *DLX1*, and *RAB38*, with ASD (Tables 2 and S11). Through real-time qPCR, we confirmed the significant upregulation of *PCDH10*, *PLXDC2*, and *SHROOM4* and the downregulation of *RAB38* (Figures 5B and 5C), but not uniformly in all affected samples. Analysis of the enriched Gene Ontology (GO) for biological processes (BPs) revealed interesting categories such as neuron differentiation (GO:0030182), cell adhesion (GO:0007155), or the positive/negative regulation of transcription from RNA polymerase II promoter (GO:0051897/GO:0000122) (Table S11).

Under ciliated conditions (−FCS), the number of DEGs increased in affected skin fibroblasts, with a significant enrichment of DEGs involved in intellectual disability ($p < 0.038$) and/or ASD ($p < 1.2E{-}06$) (Tables 2 and S12). Under this condition, the data also revealed differential expression of *GLI2*, *GLI3*, *FLNA*, and *RPGRIP1L*, four genes listed in the SYSCILIA gold standard (SCGSv1),[40] a database of known ciliary components, strengthening the hypothesis that PRMT9 might have an impact on ciliogenesis or cilia function (Table 2). To validate those results, real-time qPCR was performed on a selection of upregulated (*PCDH10*, *HCLS1*, *RPGRIP1L*, *SHROOM4*, and *FLNA*) or downregulated (*NEU1*, *BST2*, *PDK4*, and *ANGPTL4*) genes. Significance was not uniformly obtained in all affected samples. Unlike the RNA-sequencing results, *GLI3* is downregulated in the individuals of family C but not in individual A.II-1 (Figures 5B–5D). Enriched GO BPs are, e.g., actin cytoskeleton organization (GO:0030036), negative regulation of transcription, DNA-templated (GO:0045892), regulation of synaptic plasticity (GO:0048167), axon guidance (GO:0007411), cell adhesion (GO:0007155), small GTPase-mediated signal transduction (GO:0007264), and positive regulation of transcription from RNA polymerase II promoter (GO:0045944) (Table S13)

Zebrafish *MZprmt9*$^{-/-}$ mutants display abnormal social preferences

Zebrafish is an attractive model organism for studying human Mendelian diseases, such as ciliopathies[41] and

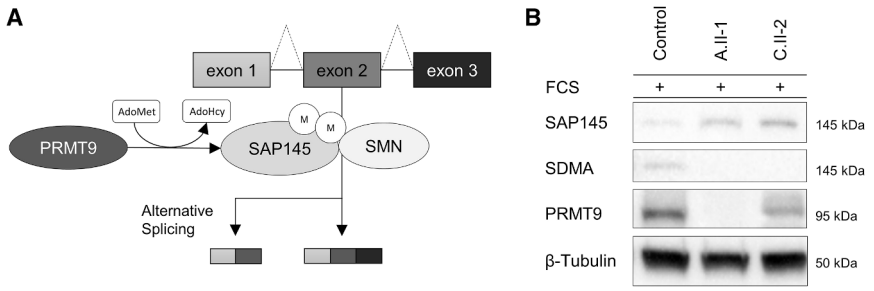

Figure 4. PRMT9 fails to methylate the splicing factor SAP145 in cells from affected individuals

(A) PRMT9 is known to symmetrically dimethylate Arg508 of SAP145 (SDMA). Due to the interaction with the splicing factor SAP145, PRMT9 was suggested to regulate alternative splicing.[10]

(B) Western blot analysis of PRMT9, SAP145, and SDMA (SAP145 dimethylated) in control and individuals' fibroblasts (A.II-1 and C.II-2) cultured under normal conditions (+FCS) ($n = 2$). β-Tubulin serves as a loading control. SAP145 signal is present in all samples but weak in control. Western blot highlights the dimethylation of SAP145 (SDMA) in control cells, while no dimethylation of SAP145 is possible in defective PRMT9 cells (i.e., no protein in A.II-1 or likely presence of a defective PRMT9 protein in C.II-2).

neurodevelopmental disorders (e.g., ASD or epilepsy).[42] *PRMT9* has a single ortholog (ENSDARG00000036755) in the zebrafish genome, located on the reverse strand of chromosome 1 with three predicted isoforms (859 aa, 876 aa, and 5 aa).[43] In this study, we considered the two longer isoforms sharing, respectively, 55% and 61% identity to the human ortholog.

We first investigated the expression of *prmt9* mRNA in zebrafish embryos by *in situ* hybridization. At 4 h post fertilization (hpf), embryos showed that *prmt9* mRNA is maternally deposited. At 24 hpf, strong *prmt9* expression was detected in the brain (cerebellum and rhombencephalon), the otic capsule, and the blood island. At 48 hpf, expression was additionally observed in the heart, epiphysis, and telencephalon (Figure 6A).

To investigate the effect of *PRMT9* LoF on the embryonic development and adult behavior of zebrafish, a CRISPR-Cas9-directed gene knockout was performed (Figure S10). We selected a guide RNA that binds a sequence within exon 4 of *prmt9* and led to an insertion of four base pairs, thus generating a frameshift and a premature stop codon (Figure S10A). This results in a putative Prmt9 protein truncated at residue 269, thus lacking functional MTase modules (Figure S10B). To exclude maternal contributions, MZ*prmt9*$^{-/-}$ mutants that lack both maternally supplied and zygotically expressed *prmt9* were analyzed. Real-time qPCR analysis of *prmt9* expression in wild type and *MZprmt9*$^{-/-\ ka709}$ mutants revealed a drastic drop of *prmt9* mRNA expression (Figure S10C), which is indicative of NMD, as was the case in cells from individual A.II-1.

Drawing from the effect on primary cilia in individuals' fibroblasts, we examined 72-hpf embryos for typical features observed in previously described zebrafish models

Table 2. Enrichment in genes involved or potentially involved in intellectual disability, ASD, or cilia function/biogenesis among the DEGs in normal and ciliary conditions

	DEGs (*n*)	Enrichment (no. of overlapping genes)	*p* value	Genes
DEGs (+FCS/normal)				
Intellectual disability ($n = 719$)	62	0.8 (2)	<0.467	*SHROOM4, SATB2*
ASD from AutismKb ($n = 1,660$)	62	1.6 (8)	<0.140	*PCDH10, HCLS1, PLXDC2, RTN1, TIPARP, CD44, DLX1, RAB38*
Cilia from SysCilia ($n = 303$)	62	0.0 (0)	<0.340	
DEGs (−FCS/ciliary condition)				
Intellectual disability ($n = 719$)	240	1.6 (16)	<0.038	*SHANK2, RAB39B, GLI2, PYCR1, PRPS1, SHROOM4, SLC1A4, FLNA, RPGRIP1L, GLI3, SYNGAP1, SPATA13, NEU1, GRM1, NEDD4L, SCN1A*
ASD from AutismKb ($n = 1,660$)	240	2.2 (43)	<1.201E−06	*SLC16A9, HCLS1, PCDH10, RTN1, PCDH7, RAB39B, MYOM2, BCAT1, ANXA2, C7orf50, PPIC, CD44, NBPF10, AHRR, SH2B2, ZNF385A, RALGPS2, GYPC, LIFR, STOM, SPATA13, H1F0, ETS2, ANKRD9, ANGPTL4, CLEC2B, ADORA2B, ITPKA, IFITM1, RHBDL3, ABCA1, PLIN2, SOD2, ATP8B4, RAB38, PDK4, NEDD4L, CMPK2, VGF, SCN1A, RSAD2, PPARGC1A, BST2*
Cilia from SysCilia ($n = 303$)	240	1.0 (4)	<0.397	*GLI2, FLNA, RPGRIP1L, GLI3*

ASD, autism spectrum disorder; DEGs, differentially expressed genes; FCS, fetal calf serum.

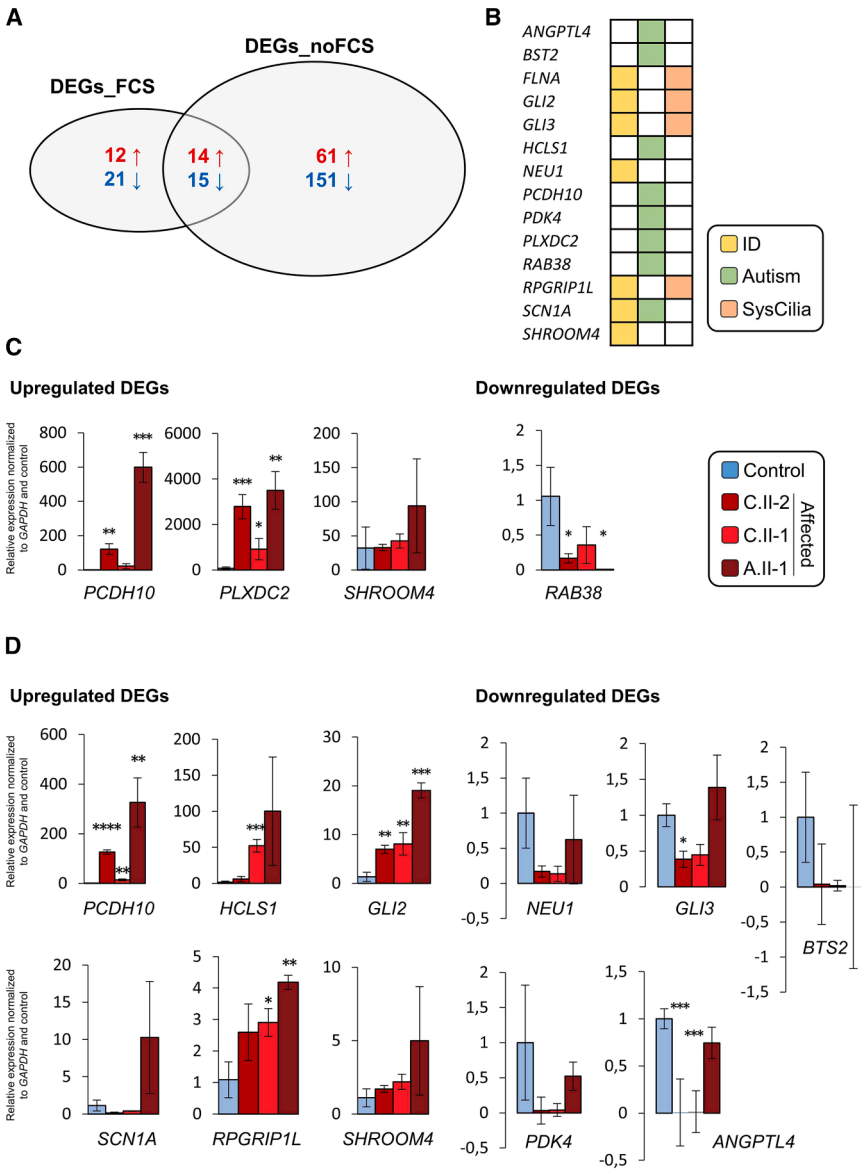

Figure 5. Multiple genes associated with intellectual disability, autism, or cilia biogenesis/function are dysregulated in individuals with bi-allelic *PRMT9* pathogenic variants

(A) Prior to RNA extraction and sequencing, control cells ($n = 3$) and individuals' fibroblasts (A.II-1, C.II-1, and C.II-2) were cultured in normal conditions (+FCS) and ciliated conditions (−FCS). To induce primary cilium formation, the cells were deprived of serum by growth for 48 h in DMEM with 1% penicillin-streptomycin. Considering only genes with a $\log_2$ fold change of <−1/>1 and an adjusted p value <0.05, 62 DEGs were identified in all three individuals in normal cell-culture conditions (+FCS), and 241 DEGs were found in ciliated conditions (−SVF), highlighting a potential role of PRMT9 during ciliogenesis.

(B) Gene category description (e.g., intellectual disability, autism, or cilia biogenesis/function) of the 14 selected out of 62 dysregulated genes further validated.

(C) Real-time qPCR analyses of the expression of upregulated and downregulated genes in the three individuals' fibroblast culture in normal conditions (+FCS) and one control.

(D) Real-time qPCR analyses of the expression of upregulated and downregulated genes in the three individuals' fibroblast culture in ciliated conditions (−FCS) and one control. Error bars represent standard deviation of biological triplicates. Statistical significance was determined using a Student's t test (*$p < 0.05$, **$p < 0.01$, ***$p < 0.001$, ****$p < 0.0001$).

of ciliopathies.[41] However, neither a curved body axis, hydrocephalus, nor kidney cysts were observed in *prmt9* mutants (Figures 6B and 6C). Furthermore, we did not observe any difference in the length of primary cilia in adult *MZprmt9*$^{-/-}$ tissue as compared to age-matched wild-type controls (Figure S11).

Since brain malformations and ASD, a feature often accompanied by brain abnormalities in both fish and humans,[44] have been described in our probands, we next examined possible morphological brain changes in MZ*prmt9* mutants. *In situ* hybridization targeting the brain markers *krox20* and *msxc* was performed on 24-hpf MZ*prmt9*-deficient embryos and wild-type embryos, but no obvious malformations of the brain structures were observed (Figure S12A). Since RNA sequencing in affected human fibroblasts revealed an abnormally high expression of *PCDH10*, a gene that participates in axon outgrowth in the forebrain of mice, we next examined the axon tracts in the forebrain of 35-hpf embryos using an antibody against acetylated tubulin. However, both wild-type and mutant *MZprmt9*$^{-/-}$ embryos exhibited intact axonal bundles, representing the main white matter tracts, in the forebrain (Figure S12B).

To test the social preference of adult animals, the swarm behavior of zebrafish can be observed. The spatial segregation of a single fish from its group, in a tank that is divided by a transparent disk, leads in general to the fact that the single fish stays most of the time close to its conspecific group.[45] In ASD models, however, zebrafish do not show this strong social behavior and swim evenly throughout their whole compartment.[29] To test the behavior of *MZprmt9*$^{-/-}$ mutants, we divided a breeding tank into two compartments with a transparent wall and placed a group of five conspecific fish on one side and a single mutant or wild-type fish on the other side (Figure 6E). While we did not observe any difference in the time spent in the conspecific sector between wild-type and *MZprmt9*$^{-/-}$ mutants, the distance traveled in the conspecific sector of the two groups differed significantly

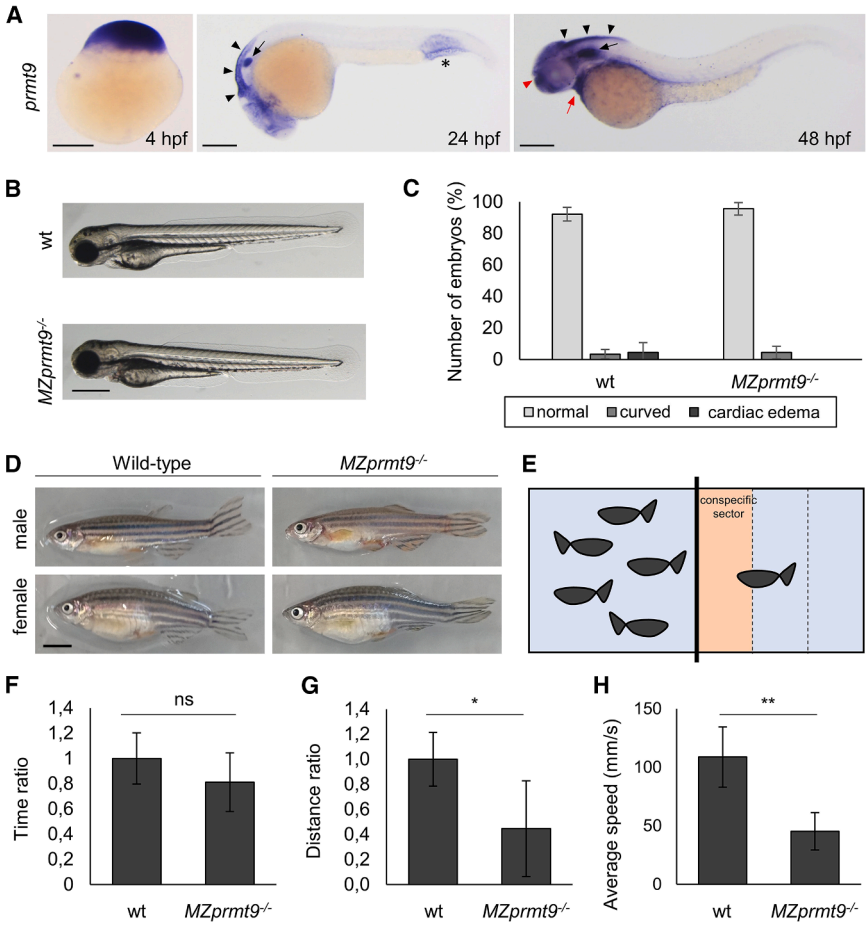

Figure 6. *MZprmt9*$^{ka709/ka709}$ mutants do not display a typical ciliopathy phenotype but show abnormal social preferences

(A) Whole-mount *in situ* hybridization analysis with *prmt9* antisense probe revealed a maternal contribution of *prmt9* mRNA (4 h post fertilization [hpf]). At 24 hpf, high expression levels of *prmt9* were detected in the hindbrain (black arrowhead), the otic capsule (black arrow), and the blood island (black asterisk). At 48 hpf, additional staining was observed in the forebrain (red arrowhead) and the heart (red arrow). Scale bars, 250 μm.

(B) Representative images of a 72-hpf wild-type (wt) and *MZprmt9*$^{ka709/ka709}$ mutant zebrafish embryo. Scale bar, 500 μm.

(C) Number of wild-type and *MZprmt9*$^{ka709/ka709}$ embryos presenting the indicated phenotype. Results are presented as percentage of the total number of analyzed animals, i.e., 122 and 178 for wild-type and mutant embryos, respectively.

(D) Representative images of adult (12 months post fertilization) wild-type and *MZprmt9*$^{ka709/ka709}$ mutant zebrafish. Scale bar, 500 μm.

(E) Schematic representation of the social behavior test.

(F) Ratio of the time spent in the conspecific sector.

(G) Ratio of the distance traveled in the conspecific sector is significantly reduced in *MZprmt9*$^{ka709/ka709}$ mutants compared to wild-type fish.

(H) The average speed of *MZprmt9*$^{ka709/ka709}$ mutants was significantly decreased in all three compartments. $n = 6$/group.
In (F)–(H), a Student's *t* test was performed to determine the significance. ns, not significant; *$p < 0.05$, **$p < 0.01$.

(Figures 6F and 6G). Mutants moved slower in all three sectors (Figure 6H) and moved less hectically in the immediate vicinity of the conspecific group (Video S1).

Discussion

PRMT9 encodes one of nine PRMTs, a protein family that can be classified into three different groups according to their methylation products. The majority of PRMTs (PRMT1, PRMT2, PRMT3, PRMT4, PRMT6, and PRMT8) can generate MMAs and asymmetric dimethylarginines (ADMAs) on their targets. Unlike type I PRMTs, PRMT9 and PRMT5 are the only members of type II PRMTs of forming MMAs and SDMAs. The sole type III member, PRMT7, only creates an MMA mark.[10] Since PRMTs have a wide spectrum of different targets, such as transcription factors, ion channels, splicing factors, scaffolding proteins, or transport proteins, it is not surprising that they have been shown to take part in many different cellular processes. For example, they have an influence on RNA splicing, tumor suppression, DNA repair, and hormone receptor signaling.[46] *PRMT9* was identified 12 years ago by homology to *PRMT7*.[47] As previously noted,[10] *PRMT9* is the official gene name for this gene located on chromosome 4 (4q31.23). It was previously referred to as *PRMT10*[7] and wrongly used for naming another intellectual-disability-associated gene, *FBXO11*, on chromosome 2 (2p16.3).[48]

In this study, we report 26 families with 35 affected individuals presenting a syndromic form of intellectual disability associated with epilepsy, autism, global developmental delay, impaired speech development, various skeletal anomalies (including polydactyly), and hypotonia. As a proven strategy for gene identification for such a heterogeneous condition,[4,49] WES has been applied worldwide to several families and, thanks to data sharing via GeneMatcher[12] or DECIPHER,[11] we were able to assemble this cohort. In 25 families, all affected individuals carry biallelic inherited variations in *PRMT9*. Of the 25 different variants, 22 were considered either likely pathogenic (class 4) or pathogenic (class 5) according to the ACMG/ClinGen classification. Given the distribution and type of identified variations (mostly truncating variant or missense in the catalytic site unable to methylate their target), we assume that LoF variations are causal of the phenotype. Interestingly, in 2011, Najmabadi and colleagues already proposed *PRMT9* (aka *PRMT10* at that

time) as a candidate isolated intellectual disability gene[7] without any other confirming report until now. The reported missense variant (p.Gly189Arg) could not be further studied. Reinvestigation of the same family (family B) shed light on additional clinical manifestations and proved the effect of the missense. A recent study obtained similar results for the same variant using *in vitro* assays (HeLa cells and plasmid constructions).[37] A second variant in the same motif (p.Gly185Glu) further highlights its functional importance. Interestingly, two other variants remain still of uncertain significance (class 3) in families K and U. The variant c.1144C>A (p.Gln382Lys) (family K) is suspected to have a splicing effect and requires RNA testing. The variant c.2405C>T (p.Thr802Ile) (family U) is strongly predicted to affect the folding of the protein. We also noticed the occurrence of the deletion of exons 6–8 in two families from Syria, suggesting a possible founder effect. In one additional family (Z-II.1), a single gain of copy of the region involving both the last exons of *PRMT9* and *TMEM184C* could be detected, while Sanger sequencing of the *PRMT9* coding sequence or WES did not reveal any other pathogenic variant in *trans* (supplemental information). Whole-genome sequencing in this individual might reveal variants in regions not covered or badly covered by WES, such as structural variations or deep intronic variations, either in *PRMT9* or in another gene.[50,51] The individual presents clinical manifestations overlapping those of other *PRMT9* individuals (global developmental delay, hypotonia, moderate intellectual disability, epilepsy with enlargement of the lateral ventricles, and bilateral fronto-parietal cortical furrows).

Regarding the clinical presentation, the 35 affected individuals described in this cohort present with a wide spectrum of neurodevelopmental phenotypes including global developmental delay with predominant language impairment and mild to severe intellectual disability, except for one individual with specific learning disability and ASD without intellectual disability. About 30% of the affected individuals have ASD. Half of them developed epilepsy. Abnormalities on brain MRI were observed in six of them and were nonspecific. Interestingly, bi-allelic variants in *PRMT7* were identified recently in more than ten individuals with mild intellectual disability, obesity, and shortening of the digits (SBIDDS [MIM: 617157]).[52,53] Our cohort has several overlapping clinical features with this condition besides obvious intellectual disability such as the skeletal phenotype with short stature, digit anomalies (short, brachydactyly), strabismus, and urogenital anomalies, albeit in a limited number of families. Although dysmorphic facial features were noted for most of the individuals, this seems not very specific but includes shared features with flat facial profile, prominent forehead and frontal bossing, thick eyebrows, hypertelorism, and thin lips. Considering the presence of postaxial polydactyly, cryptorchidism as well as unconfirmed retinal degeneration in the index family pointed us to a possible role of PRMT9 in the biogenesis or function of the cilia. Interestingly, two independent proteomic analyses revealed PRMT5 as a primary cilia candidate where kidney mice cells or swine choroid plexus epithelial cells were isolated using a calcium-shock method.[54,55] Similarly, orthologs of the human PRMT1, PRMT3, and PRMT5 were detected in a punctate pattern along the length and on the tip of flagella or were enriched at the base of the flagella in *Chlamydomonas reinhardtii*, suggesting that these PRMTs are cargo of the intraflagellar transport.[56] PRMT1 was shown to methylate GLI1 in the cytoplasm of pancreatic ductal adenocarcinoma but does not interfere with the Shh pathway.[57] Moreover, PRMT5 associated with MEP50 was shown to stabilize GLI1 through methylation of different arginine residues and promote GLI1 activation via the Shh pathway.[58] More recently, PRMT7 was shown to interact with and methylate GLI2, facilitating the release of GLI2 from SUFU its negative regulator in the Shh pathway.[59] PRMT9 contains three TPR domains well known to be involved in protein-protein interactions in large complexes and which are found in many ciliary-related proteins, especially in the intraflagellar transport machinery.[60,61] However, no cilia localization of PRMT9 could be shown either in our hands (data not shown) or in the literature. This result does not exclude the possibility that PRMT9 is involved in the biogenesis/functioning of the cilia, since other ciliopathy-associated genes, for example *LZTFL1*, are also not localized in the cilia.[62] Moreover, in this study we were able to show that primary cilia are significantly longer in individuals' cells with *PRMT9* LoF variations compared to controls and demonstrated Shh pathway dysregulation with two of the main component and target genes significantly overexpressed. Interestingly, these observations were identical whether using either a fully depleted PRMT9 cell (absence of protein for A.II-1) or a half reduced amount of PRMT9 and a defective PRMT9 protein (C.II-1 and C.II-2). Transcriptomic analysis and subsequent RT-qPCR experiments revealed a significant upregulation of *GLI2* and *RPGRIP1L* in affected fibroblasts under serum-starved conditions. Variations in *RPGRIP1L* are known to cause ciliopathies associated with strong brain anomalies, such as Joubert syndrome (JBTS7 [MIM: 611560]) and Meckel-Gruber syndrome (MKS5 [MIM: 611561]). RPGRIP1L localizes to the ciliary transition zone at the base of the basal body and is responsible for the organized entrance and exit of proteins. Primary cilia have been shown to play an important role in forebrain patterning via the regulation of the Shh pathway, in which GLI2 plays a key role.[63] The regulated expression of both *RPGRIP1L* and *GLI2* is essential for the function of primary cilia and the development of the forebrain.[63] It might be too soon to categorize *PRMT9* within the ciliopathy range; further explorations of the protein function and localization are required to see whether it can be considered as a first- or second-order ciliopathy-related gene.[64] Interestingly, many intellectual-disability-associated genes are

known to be implicated in either cilia or centrosome functions.[5]

Furthermore, due to the strong interaction of PRMT9 with the splice factor SAP145, PRMT9 was suggested to regulate alternative splicing. A protein complex consisting of PRMT9, SAP145, and SAP49 is most likely formed in the cytoplasm and followed by the dimethylation of SAP145 through PRMT9, its primary substrate.[37] SAP145 as well as SAP49 are core components of the nuclear U2 small nuclear ribonucleoprotein that is involved in splicing and 3′ processing of pre-mRNAs.[10] To find targets of PRMT9-regulated splicing, Yang and colleagues compared RNA-sequencing data of control knockdown and small interfering RNA-mediated PRMT9 knockdown HeLa cells and identified splice variants in several intellectual-disability-associated genes such as *NDUFS2*, *WAC*, *BCOR*, and *EEF1B2* by RNA sequencing.[5,10] We were unable to replicate these findings, suggesting that PRMT9-associated alternative splicing might vary between tissues and cell types. Several splicing events could be identified in our dataset but with a high rate of false positives after careful examination of the sequencing data; thus, no significant event could be reported.

In addition, the investigation of DEGs in both serum rich (+FCS) and ciliated (−FCS) conditions gave hints as to which pathways linked to intellectual disability and autism PRMT9 might be involved. We observed an increase of DEGs in individuals' fibroblasts cultured in serum-starved conditions (−FCS) compared to serum-rich conditions (+FCS), highlighting a potential role of PRMT9 during ciliogenesis. Overall, we observed a large number of DEGs associated with intellectual disability and autism, such as *SHROOM4*, *SATB2*, *RB38*, or *SHANK2*,[3,39,65] in both cell-culture conditions. Among others, the most highly overexpressed gene is *PCDH10* that encodes a cadherin superfamily protein normally expressed in the basolateral amygdala, a brain region implicated in autistically relevant behavior.[66,67] The *pcdh10*$^{-/-}$ in mouse has been shown to be crucial for axon outgrowth in the forebrain,[68] and homozygous deletions of the human *PCDH10* have been identified in autistic children.[69]

We also observed an enrichment of DEGs in individuals' cells (in both serum-rich and ciliated conditions) implicated in biological processes linked to autism and intellectual disability. In +FCS conditions, for example, six DEGs (*AMBP*, *CD44*, *PCDH10*, *COL28A1*, *CDH4*, and *THBS4*) associated with cell adhesion were identified. Synaptic cell adhesion molecules are involved in cell-cell recognition during synapse formation and are strongly associated with intellectual disability and autism. Another enriched GO term was the negative regulation of transcription from RNA polymerase II promoter (DEGs: *MDFI*, *MSX2*, *HHEX*, *DLX1*, *SATB2*, *DACT1*, and *HCLS1*). In the past many genes implicated in transcriptional regulation, such as transcription factors and chromatin modifiers, have been associated with intellectual disability and autism.[70] The transcription factor *SATB2*, for example, is strongly associated with intellectual disability and autism.[65,71] In addition to the enriched GO terms in +FCS conditions, in ciliary conditions the enrichment of genes involved in the actin cytoskeleton organization (DEGs *GAS2L3*, *RND3*, *SHROOM4*, *TESK2*, *SH2B2*, *ITPKA*, and *FGD4*), the regulation of synaptic plasticity (DEGs *LZTS1*, *SYNGAP1*, *VGF*, and *ITPKA*) and small GTPase-mediated signal transduction (DEGs *RND3*, *RAB32*, *RALGPS2*, *PLCE1*, *RAB39B*, *RAB38*, *DOCK11*, and *DOCK4*) was observed. The cytoskeleton gives neurons its shape and stabilizes the entire cell. Moreover, the cytoskeletal organization is important during axon outgrowth and synapse formation and is thus important for remodeling of synaptic connections.[72] Also, genes involved in the GTPase signaling pathway have been implicated in the organization of the actin cytoskeleton and hence have an impact on the structure and function of dendrites and synapses.[73] Moreover, they are implicated in the intracellular vesicle trafficking in neurons, such as RAB39B.[73,74]

Brain study of MZ*prmt9*$^{-/-}$ mutant zebrafish larvae did not reveal any obvious difference compared to wild type, and they reached adulthood normally. However, this does not exclude that subtle modifications occur at later stages. More investigation would be required in order to map the different brain areas of the adult to detect anomalies. Differently from individuals' skin fibroblasts, the size of the primary cilia was not affected in MZ*prmt9*$^{-/-}$ zebrafish. The mutation within *prmt9* leads to NMD, which was shown to frequently trigger genetic compensation.[75] One cannot exclude that another gene takes over the role of *prmt9* to minimize the effect of the deletion. To this end, transcriptomic analysis could reveal the overexpression of compensatory genes, thereby providing insights into the molecular pathways involved in the disease. In addition, differences between wild-type and mutant behavioral activities indicate a link between *PRMT9* and ASD. Although the time spent in the conspecific sector did not differ from wild-type fish, MZ*prmt9*$^{-/-}$ mutants showed a dramatic decrease in velocity, a behavior previously observed in zebrafish models of autism, such as *shank3b*$^{-/-}$ mutants or *syngap1b* morphants.[29,76] This phenotype is most likely not due to a general motility defect. Indeed, we did not observe any difference in brain development and in axon tracts, in particular for motoneurons between MZ*prmt9*$^{-/-}$ larvae and wild-type siblings, and muscle integrity was not affected in the mutant (Figure S13). Furthermore, heterozygous crosses gave rise to a normal Mendelian ratio of homozygous mutants that were able to reach adulthood (not shown). This shows that mutant larvae raised in a tank were able to compete for food with wild-type siblings, which is strongly indicative of the absence of a motility defect. Finally, the general swimming behavior of adult mutant fish (escape from capture net and food catching) was not different from that of wild-type fish (not shown). Developing a *prmt9* zebrafish model for

one of the identified missense variants would be very interesting, as this is described to be less prone to genetic compensation[75] and thus could result in a more drastic phenotype.

In conclusion, we have identified bi-allelic pathogenic variants in *PRMT9* in a large cohort of individuals ($n = 35$), confirming *PRMT9* as a syndromic autosomal-recessive intellectual-disability-associated gene. The variations affect PRMT9 function in dimethylating its partner and suggest a role for PRMT9 in cilia biogenesis and function.

Data and code availability

Data generated or analyzed during this study are included in the published article and the corresponding supplemental information. The raw sequencing data generated in the course of this study are not publicly available due to the protocol and the corresponding consents used that did not include such information. All variants have been submitted to ClinVar using the range of accessions numbers SCV002569976 to SCV002569999 (https://www.ncbi.nlm.nih.gov/clinvar/). Coordinates and structure factors for Apo-PRMT9 have been deposited in the Protein Data Bank under the accession code PDB: 6PDM. The *prmt9* zebrafish mutant is available in the European Zebrafish Resources Centre (https://www.ezrc.kit.edu) and in the Zebrafish Information Network (ZFIN, https://zfin.org/ZDB-ALT-251002-3) under the laboratory designation ka735.

Acknowledgments

We thank the families for their participation and collaboration. Additional acknowledgments are available in the supplemental information.

Author contributions

E.S., S.S., K.K., J.P., A.F., N.M., M.A.A.C., K.C.A., L.R., J.L., B.D., A.-C.T., I.M.W., T.S.-S., R.Y., M.F.S., E.A., C.L., S.B.W., R.G.F., J.A.M., H.G., G.J., X.W., J.W., T.B., L.G., T.H., A.R., E.G., A. Kampmeier, A. Kuechler, K.P., R.A.J., A.W., M.I., S.G.K., F.L., V.T., C.M.K., F.H., L.L.P.R., F.K., C.B.B., I.M.B.H.v.d.L., S.A.d.M., E.T., A.S., A.B., Z.Y., S.S.C., C.C., F.T.M.T., E.L., T.C., D.H., S.W., J.R., A.v.H., H.N., and H.D. gathered data from affected individuals and performed clinical investigations; A.K.-H., C.S., V.G., A.F., K.T., N.M., C.O., F.L., G.C., I.W., T.S.-S., M.P., L.R., A.G., B.K., H.N., J.W., Y.Y., and X.W. performed molecular biology and cellular experiments or analysis including Sanger and next-generation sequencing data analysis, qPCR, western blots, and skin fibroblast analysis; A.K.-H., D.P., C.K., F.M., and A.P. performed the RNA-sequencing analysis; L.H., H.Z., C.K.A., and C.H.A. assembled and analyzed the 3D structure; A.K.-H., C.E., O.K., and U.S. designed and performed the zebrafish experiments and data analyses; A.K.-H., C.S., C.E., L.H., and J.M. analyzed the data and wrote the paper; and C.H.A., U.S., H.D., and J.M. provided direction for the project and conceived and designed the experiments. All authors approved the manuscript.

Declaration of interests

I.M.W. and T.S.-S. are employees of GeneDx, Inc.

Supplemental information

Supplemental information can be found online at https://doi.org/10.1016/j.ajhg.2025.10.014.

Web resources

ClinVar, https://www.ncbi.nlm.nih.gov/clinvar/
DAVID, https://davidbioinformatics.nih.gov/
dbSNP, https://www.ncbi.nlm.nih.gov/projects/SNP/
DECIPHER, https://decipher.sanger.ac.uk/
ENCODE, https://www.encodeproject.org/
EZRC, https://itgmv3.itg.kit.edu/ffdb/index.html
GeneMatcher, https://genematcher.org/
Gene Ontology (GO), http://geneontology.org/
gnomAD, https://gnomad.broadinstitute.org/
HGNC, https://www.genenames.org/
HGVS nomenclature, http://www.hgvs.org/mutnomen/recs.html/
Human Protein Atlas (HPA), http://www.proteinatlas.org/
Integrative Genomics Viewer (IGV), https://www.broadinstitute.org/igv/
OMIM, http://www.omim.org/
Protein Data Bank (PDB), https://www.pdb.org/
SysID database, https://sysid.cmbi.umcn.nl/
UCSC, http://genome.ucsc.edu/

Received: July 22, 2024
Accepted: October 28, 2025
Published: November 18, 2025

References

1. Maulik, P.K., Mascarenhas, M.N., Mathers, C.D., Dua, T., and Saxena, S. (2011). Prevalence of intellectual disability: A meta-analysis of population-based studies. Res. Dev. Disabil. *32*, 419–436. https://doi.org/10.1016/j.ridd.2010.12.018.
2. Doble, B., Schofield, D., Evans, C.-A., Groza, T., Mattick, J.S., Field, M., and Roscioli, T. (2020). Impacts of genomics on the health and social costs of intellectual disability. J. Med. Genet. *57*, 479–486. https://doi.org/10.1136/jmedgenet-2019-106445.
3. Vissers, L.E.L.M., Gilissen, C., and Veltman, J.A. (2016). Genetic studies in intellectual disability and related disorders. Nat. Rev. Genet. *17*, 9–18. https://doi.org/10.1038/nrg3999.
4. Gilissen, C., Hehir-Kwa, J.Y., Thung, D.T., van de Vorst, M., van Bon, B.W.M., Willemsen, M.H., Kwint, M., Janssen, I.M., Hoischen, A., Schenck, A., et al. (2014). Genome sequencing identifies major causes of severe intellectual disability. Nature *511*, 344–347.
5. Kochinke, K., Zweier, C., Nijhof, B., Fenckova, M., Cizek, P., Honti, F., Keerthikumar, S., Oortveld, M.A.W., Kleefstra, T., Kramer, J.M., et al. (2016). Systematic Phenomics Analysis Deconvolutes Genes Mutated in Intellectual Disability into Biologically Coherent Modules. Am. J. Hum. Genet. *98*, 149–164. https://doi.org/10.1016/j.ajhg.2015.11.024.
6. Jamra, R. (2018). Genetics of autosomal recessive intellectual disability. Med. Genet. *30*, 323–327. https://doi.org/10.1007/s11825-018-0209-z.
7. Najmabadi, H., Hu, H., Garshasbi, M., Zemojtel, T., Abedini, S.S., Chen, W., Hosseini, M., Behjati, F., Haas, S., Jamali, P., et al. (2011). Deep sequencing reveals 50 novel genes for

recessive cognitive disorders. Nature *478*, 57–63. https://doi.org/10.1038/nature10423.
8. Anvarian, Z., Mykytyn, K., Mukhopadhyay, S., Pedersen, L.B., and Christensen, S.T. (2019). Cellular signalling by primary cilia in development, organ function and disease. Nat. Rev. Nephrol. *15*, 199–219. https://doi.org/10.1038/s41581-019-0116-9.
9. Valente, E.M., Rosti, R.O., Gibbs, E., and Gleeson, J.G. (2014). Primary cilia in neurodevelopmental disorders. Nat. Rev. Neurol. *10*, 27–36. https://doi.org/10.1038/nrneurol.2013.247.
10. Yang, Y., Hadjikyriacou, A., Xia, Z., Gayatri, S., Kim, D., Zurita-Lopez, C., Kelly, R., Guo, A., Li, W., Clarke, S.G., and Bedford, M.T. (2015). PRMT9 is a type II methyltransferase that methylates the splicing factor SAP145. Nat. Commun. *6*, 6428. https://doi.org/10.1038/ncomms7428.
11. Firth, H.V., Richards, S.M., Bevan, A.P., Clayton, S., Corpas, M., Rajan, D., Van Vooren, S., Moreau, Y., Pettett, R.M., and Carter, N.P. (2009). DECIPHER: Database of Chromosomal Imbalance and Phenotype in Humans Using Ensembl Resources. Am. J. Hum. Genet. *84*, 524–533. https://doi.org/10.1016/j.ajhg.2009.03.010.
12. Sobreira, N., Schiettecatte, F., Valle, D., and Hamosh, A. (2015). GeneMatcher: a matching tool for connecting investigators with an interest in the same gene. Hum. Mutat. *36*, 928–930. https://doi.org/10.1002/humu.22844.
13. Scheidecker, S., Etard, C., Pierce, N.W., Geoffroy, V., Schaefer, E., Muller, J., Chennen, K., Flori, E., Pelletier, V., Poch, O., et al. (2014). Exome sequencing of Bardet–Biedl syndrome patient identifies a null mutation in the BBSome subunit *BBIP1* (*BBS18*). J. Med. Genet. *51*, 132–136. https://doi.org/10.1136/jmedgenet-2013-101785.
14. Hutchinson, A., and Seitova, A. (2021). Production of recombinant PRMT proteins using the baculovirus expression vector system. J. Vis. Exp. https://doi.org/10.3791/62510.
15. Kabsch, W. (2010). XDS. Acta Crystallogr. D Biol. Crystallogr. *66*, 125–132. https://doi.org/10.1107/S0907444909047337.
16. Terwilliger, T.C., DiMaio, F., Read, R.J., Baker, D., Bunkóczi, G., Adams, P.D., Grosse-Kunstleve, R.W., Afonine, P.V., and Echols, N. (2012). phenix.mr_rosetta: molecular replacement and model rebuilding with Phenix and Rosetta. J. Struct. Funct. Genomics *13*, 81–90. https://doi.org/10.1007/s10969-012-9129-3.
17. Emsley, P., Lohkamp, B., Scott, W.G., and Cowtan, K. (2010). Features and development of *Coot*. Acta Crystallogr. D Biol. Crystallogr. *66*, 486–501. https://doi.org/10.1107/S0907444910007493.
18. Bricogne, G., Blanc, E., Brandl, M., Flensburg, C., Keller, P., Paciorek, W., Roversi, P., Sharff, A., Smart, O.S., Vonrhein, C., and Womack, T.O. (2017). Buster Version 2.10.2 (Cambridge, United Kingdom: Global Phasing Ltd).
19. Williams, C.J., Headd, J.J., Moriarty, N.W., Prisant, M.G., Videau, L.L., Deis, L.N., Verma, V., Keedy, D.A., Hintze, B.J., Chen, V.B., et al. (2018). MolProbity: More and better reference data for improved all-atom structure validation: PROTEIN SCIENCE.ORG. Protein Sci. *27*, 293–315. https://doi.org/10.1002/pro.3330.
20. Schrödinger LLC (2015). The PyMOL Molecular Graphics System, version 1.8
21. Estrada-Cuzcano, A., Etard, C., Delvallée, C., Stoetzel, C., Schaefer, E., Scheidecker, S., Geoffroy, V., Schneider, A., Studer, F., Mattioli, F., et al. (2020). Novel IQCE variations confirm its role in postaxial polydactyly and cause ciliary defect phenotype in zebrafish. Hum. Mutat. *41*, 240–254. https://doi.org/10.1002/humu.23924.
22. Aranda, P.S., LaJoie, D.M., and Jorcyk, C.L. (2012). Bleach gel: a simple agarose gel for analyzing RNA quality. Electrophoresis *33*, 366–369. https://doi.org/10.1002/elps.201100335.
23. Etard, C., Joshi, S., Stegmaier, J., Mikut, R., and Strähle, U. (2017). Tracking of Indels by DEcomposition is a Simple and Effective Method to Assess Efficiency of Guide RNAs in Zebrafish. Zebrafish *14*, 586–588. https://doi.org/10.1089/zeb.2017.1454.
24. Aleström, P., D'Angelo, L., Midtlyng, P.J., Schorderet, D.F., Schulte-Merker, S., Sohm, F., and Warner, S. (2020). Zebrafish: Housing and husbandry recommendations. Lab. Anim. *54*, 213–224. https://doi.org/10.1177/0023677219869037.
25. Kimmel, C.B., Ballard, W.W., Kimmel, S.R., Ullmann, B., and Schilling, T.F. (1995). Stages of embryonic development of the zebrafish. Dev. Dyn. *203*, 253–310. https://doi.org/10.1002/aja.1002030302.
26. Yang, L., Rastegar, S., and Strähle, U. (2010). Regulatory interactions specifying Kolmer-Agduhr interneurons. Development *137*, 2713–2722. https://doi.org/10.1242/dev.048470.
27. Armant, O., März, M., Schmidt, R., Ferg, M., Diotel, N., Ertzer, R., Bryne, J.C., Yang, L., Baader, I., Reischl, M., et al. (2013). Genome-wide, whole mount in situ analysis of transcriptional regulators in zebrafish embryos. Dev. Biol. *380*, 351–362. https://doi.org/10.1016/j.ydbio.2013.05.006.
28. Middel, V., Zhou, L., Takamiya, M., Beil, T., Shahid, M., Roostalu, U., Grabher, C., Rastegar, S., Reischl, M., Nienhaus, G.U., and Strähle, U. (2016). Dysferlin-mediated phosphatidylserine sorting engages macrophages in sarcolemma repair. Nat. Commun. *7*, 12875. https://doi.org/10.1038/ncomms12875.
29. Liu, C.X., Li, C.Y., Hu, C.C., Wang, Y., Lin, J., Jiang, Y.H., Li, Q., and Xu, X. (2018). CRISPR/Cas9-induced shank3b mutant zebrafish display autism-like behaviors. Mol. Autism *9*, 23. https://doi.org/10.1186/s13229-018-0204-x.
30. Rodriguez, A., Zhang, H., Klaminder, J., Brodin, T., Andersson, P.L., and Andersson, M. (2018). *ToxTrac* : A fast and robust software for tracking organisms. Methods Ecol. Evol. *9*, 460–464. https://doi.org/10.1111/2041-210X.12874.
31. Rodriguez, A., Zhang, H., Klaminder, J., Brodin, T., and Andersson, M. (2017). ToxId: an efficient algorithm to solve occlusions when tracking multiple animals. Sci. Rep. *7*, 14774. https://doi.org/10.1038/s41598-017-15104-2.
32. Sjöstedt, E., Zhong, W., Fagerberg, L., Karlsson, M., Mitsios, N., Adori, C., Oksvold, P., Edfors, F., Limiszewska, A., Hikmet, F., et al. (2020). An atlas of the protein-coding genes in the human, pig, and mouse brain. Science *367*, eaay5947. https://doi.org/10.1126/science.aay5947.
33. Yang, Y., Hadjikyriacou, A., Xia, Z., Gayatri, S., Kim, D., Zurita-Lopez, C., Kelly, R., Guo, A., Li, W., Clarke, S.G., and Bedford, M.T. (2015). PRMT9 is a Type II methyltransferase that methylates the splicing factor SAP145. Nat. Commun. *6*, 6428. https://doi.org/10.1038/ncomms7428.
34. Tewary, S.K., Zheng, Y.G., and Ho, M.-C. (2019). Protein arginine methyltransferases: insights into the enzyme structure and mechanism at the atomic level. Cell. Mol. Life Sci. *76*, 2917–2932. https://doi.org/10.1007/s00018-019-03145-x.
35. Cura, V., Troffer-Charlier, N., Wurtz, J.-M., Bonnefond, L., and Cavarelli, J. (2014). Structural insight into arginine methylation by the mouse protein arginine methyltransferase 7: a

zinc finger freezes the mimic of the dimeric state into a single active site. Acta Crystallogr. D Biol. Crystallogr. *70*, 2401–2412. https://doi.org/10.1107/S1399004714014278.

36. Jurrus, E., Engel, D., Star, K., Monson, K., Brandi, J., Felberg, L.E., Brookes, D.H., Wilson, L., Chen, J., Liles, K., et al. (2018). Improvements to the APBS biomolecular solvation software suite: Improvements to the APBS Software Suite. Protein Sci. *27*, 112–128. https://doi.org/10.1002/pro.3280.
37. Shen, L., Ma, X., Wang, Y., Wang, Z., Zhang, Y., Pham, H.Q.H., Tao, X., Cui, Y., Wei, J., Lin, D., et al. (2024). Loss-of-function mutation in PRMT9 causes abnormal synapse development by dysregulation of RNA alternative splicing. Nat. Commun. *15*, 2809. https://doi.org/10.1038/s41467-024-47107-9.
38. Harripaul, R., Vasli, N., Mikhailov, A., Rafiq, M.A., Mittal, K., Windpassinger, C., Sheikh, T.I., Noor, A., Mahmood, H., Downey, S., et al. (2018). Mapping autosomal recessive intellectual disability: combined microarray and exome sequencing identifies 26 novel candidate genes in 192 consanguineous families. Mol. Psychiatry *23*, 973–984. https://doi.org/10.1038/mp.2017.60.
39. Xu, L.-M., Li, J.-R., Huang, Y., Zhao, M., Tang, X., and Wei, L. (2012). AutismKB: an evidence-based knowledgebase of autism genetics. Nucleic Acids Res. *40*, D1016–D1022. https://doi.org/10.1093/nar/gkr1145.
40. van Dam, T.J., Wheway, G., Slaats, G.G., SYSCILIA Study Group, Huynen, M.A., and Giles, R.H. (2013). The SYSCILIA gold standard (SCGSv1) of known ciliary components and its applications within a systems biology consortium. Cilia *2*, 7. https://doi.org/10.1186/2046-2530-2-7.
41. Song, Z., Zhang, X., Jia, S., Yelick, P.C., and Zhao, C. (2016). Zebrafish as a Model for Human Ciliopathies. Journal of Genetics and Genomics *43*, 107–120. https://doi.org/10.1016/j.jgg.2016.02.001.
42. Vaz, R., Hofmeister, W., and Lindstrand, A. (2019). Zebrafish Models of Neurodevelopmental Disorders: Limitations and Benefits of Current Tools and Techniques. Int. J. Mol. Sci. *20*, 1296. https://doi.org/10.3390/ijms20061296.
43. Zerbino, D.R., Achuthan, P., Akanni, W., Amode, M.R., Barrell, D., Bhai, J., Billis, K., Cummins, C., Gall, A., Girón, C.G., et al. (2018). Ensembl 2018. Nucleic Acids Res. *46*, D754–D761. https://doi.org/10.1093/nar/gkx1098.
44. Elsen, G.E., Choi, L.Y., Prince, V.E., and Ho, R.K. (2009). The autism susceptibility gene met regulates zebrafish cerebellar development and facial motor neuron migration. Dev. Biol. *335*, 78–92. https://doi.org/10.1016/j.ydbio.2009.08.024.
45. Meshalkina, D.A., N Kizlyk, M., V Kysil, E., Collier, A.D., Echevarria, D.J., Abreu, M.S., Barcellos, L.J.G., Song, C., Warnick, J.E., Kyzar, E.J., and Kalueff, A.V. (2018). Zebrafish models of autism spectrum disorder. Exp. Neurol. *299*, 207–216. https://doi.org/10.1016/j.expneurol.2017.02.004.
46. Morales, Y., Cáceres, T., May, K., and Hevel, J.M. (2016). Biochemistry and regulation of the protein arginine methyltransferases (PRMTs). Arch. Biochem. Biophys. *590*, 138–152. https://doi.org/10.1016/j.abb.2015.11.030.
47. Krause, C.D., Yang, Z.-H., Kim, Y.-S., Lee, J.-H., Cook, J.R., and Pestka, S. (2007). Protein arginine methyltransferases: Evolution and assessment of their pharmacological and therapeutic potential. Pharmacol. Ther. *113*, 50–87. https://doi.org/10.1016/j.pharmthera.2006.06.007.
48. Jansen, S., van der Werf, I.M., Innes, A.M., Afenjar, A., Agrawal, P.B., Anderson, I.J., Atwal, P.S., van Binsbergen, E., van den Boogaard, M.-J., Castiglia, L., et al. (2019). De novo variants in FBXO11 cause a syndromic form of intellectual disability with behavioral problems and dysmorphisms. Eur. J. Hum. Genet. *27*, 738–746. https://doi.org/10.1038/s41431-018-0292-2.
49. Snoeijen-Schouwenaars, F.M., van Ool, J.S., Verhoeven, J.S., van Mierlo, P., Braakman, H.M.H., Smeets, E.E., Nicolai, J., Schoots, J., Teunissen, M.W.A., Rouhl, R.P.W., et al. (2019). Diagnostic exome sequencing in 100 consecutive patients with both epilepsy and intellectual disability. Epilepsia *60*, 155–164. https://doi.org/10.1111/epi.14618.
50. Geoffroy, V., Stoetzel, C., Scheidecker, S., Schaefer, E., Perrault, I., Bär, S., Kröll, A., Delbarre, M., Antin, M., Leuvrey, A.-S., et al. (2018). Whole-genome sequencing in patients with ciliopathies uncovers a novel recurrent tandem duplication in IFT140. Hum. Mutat. *39*, 983–992. https://doi.org/10.1002/humu.23539.
51. Kröll-Hermi, A., Ebstein, F., Stoetzel, C., Geoffroy, V., Schaefer, E., Scheidecker, S., Bär, S., Takamiya, M., Kawakami, K., Zieba, B.A., et al. (2020). Proteasome subunit PSMC3 variants cause neurosensory syndrome combining deafness and cataract due to proteotoxic stress. EMBO Mol. Med. *12*, e11861. https://doi.org/10.15252/emmm.201911861.
52. Birnbaum, R., Yosha-Orpaz, N., Yanoov-Sharav, M., Kidron, D., Gur, H., Yosovich, K., Lerman-Sagie, T., Malinger, G., and Lev, D. (2019). Prenatal and postnatal presentation of PRMT7 related syndrome: Expanding the phenotypic manifestations. Am. J. Med. Genet. *179*, 78–84. https://doi.org/10.1002/ajmg.a.6.
53. Poquérusse, J., Whitford, W., Taylor, J., Alburaiky, S., Snell, R.G., Lehnert, K., and Jacobsen, J.C. (2022). Novel PRMT7 mutation in a rare case of dysmorphism and intellectual disability. J. Hum. Genet. *67*, 19–26. https://doi.org/10.1038/s10038-021-00955-5.
54. Ishikawa, H., Thompson, J., Yates, J.R., and Marshall, W.F. (2012). Proteomic Analysis of Mammalian Primary Cilia. Curr. Biol. *22*, 414–419. https://doi.org/10.1016/j.cub.2012.01.031.
55. Narita, K., Kozuka-Hata, H., Nonami, Y., Ao-Kondo, H., Suzuki, T., Nakamura, H., Yamakawa, K., Oyama, M., Inoue, T., and Takeda, S. (2012). Proteomic analysis of multiple primary cilia reveals a novel mode of ciliary development in mammals. Biol. Open *1*, 815–825. https://doi.org/10.1242/bio.20121081.
56. Mizuno, K., and Sloboda, R.D. (2017). Protein arginine methyltransferases interact with intraflagellar transport particles and change location during flagellar growth and resorption. Mol. Biol. Cell *28*, 1208–1222. https://doi.org/10.1091/mbc.e16-11-0774.
57. Wang, Y., Hsu, J.-M., Kang, Y., Wei, Y., Lee, P.-C., Chang, S.-J., Hsu, Y.-H., Hsu, J.L., Wang, H.-L., Chang, W.-C., et al. (2016). Oncogenic Functions of Gli1 in Pancreatic Adenocarcinoma Are Supported by Its PRMT1-Mediated Methylation. Cancer Res. *76*, 7049–7058. https://doi.org/10.1158/0008-5472.CAN-16-0715.
58. Abe, Y., Suzuki, Y., Kawamura, K., and Tanaka, N. (2019). MEP50/PRMT5-mediated methylation activates GLI1 in Hedgehog signalling through inhibition of ubiquitination by the ITCH/NUMB complex. Commun. Biol. *2*, 23. https://doi.org/10.1038/s42003-018-0275-4.
59. Vuong, T.A., Jeong, H.-J., Lee, H.-J., Kim, B.-G., Leem, Y.-E., Cho, H., and Kang, J.-S. (2020). PRMT7 methylates and

suppresses GLI2 binding to SUFU thereby promoting its activation. Cell Death Differ. *27*, 15–28. https://doi.org/10.1038/s41418-019-0334-5.

60. Taschner, M., Bhogaraju, S., and Lorentzen, E. (2012). Architecture and function of IFT complex proteins in ciliogenesis. Differentiation. *83*, S12–S22. https://doi.org/10.1016/j.diff.2011.11.001.
61. Xu, Y., Cao, J., Huang, S., Feng, D., Zhang, W., Zhu, X., and Yan, X. (2015). Characterization of Tetratricopeptide Repeat-Containing Proteins Critical for Cilia Formation and Function. PLoS One *10*, e0124378. https://doi.org/10.1371/journal.pone.0124378.
62. Eguether, T., San Agustin, J.T., Keady, B.T., Jonassen, J.A., Liang, Y., Francis, R., Tobita, K., Johnson, C.A., Abdelhamed, Z.A., Lo, C.W., and Pazour, G.J. (2014). IFT27 Links the BBSome to IFT for Maintenance of the Ciliary Signaling Compartment. Dev. Cell *31*, 279–290. https://doi.org/10.1016/j.devcel.2014.09.011.
63. Andreu-Cervera, A., Anselme, I., Karam, A., Laclef, C., Catala, M., and Schneider-Maunoury, S. (2019). The ciliopathy gene ftm/rpgrip1l controls mouse forebrain patterning via region-specific modulation of hedgehog/gli signaling. J. Neurosci. *39*, 2398–2415. https://doi.org/10.1523/JNEUROSCI.2199-18.2019.
64. Reiter, J.F., and Leroux, M.R. (2017). Genes and molecular pathways underpinning ciliopathies. Nat. Rev. Mol. Cell Biol. *18*, 533–547. https://doi.org/10.1038/nrm.2017.60.
65. Talkowski, M.E., Rosenfeld, J.A., Blumenthal, I., Pillalamarri, V., Chiang, C., Heilbut, A., Ernst, C., Hanscom, C., Rossin, E., Lindgren, A.M., et al. (2012). Sequencing chromosomal abnormalities reveals neurodevelopmental loci that confer risk across diagnostic boundaries. Cell *149*, 525–537. https://doi.org/10.1016/j.cell.2012.03.028.
66. Hirano, S., Yan, Q., and Suzuki, S.T. (1999). Expression of a Novel Protocadherin, OL-Protocadherin, in a Subset of Functional Systems of the Developing Mouse Brain. J. Neurosci. *19*, 995–1005. https://doi.org/10.1523/JNEUROSCI.19-03-00995.1999.
67. Wang, X., Guo, J., Song, Y., Wang, Q., Hu, S., Gou, L., and Gao, Y. (2018). Decreased Number and Expression of nNOS-Positive Interneurons in Basolateral Amygdala in Two Mouse Models of Autism. Front. Cell. Neurosci. *12*, 251. https://doi.org/10.3389/fncel.2018.00251.
68. Uemura, M., Nakao, S., Suzuki, S.T., Takeichi, M., and Hirano, S. (2007). OL-protocadherin is essential for growth of striatal axons and thalamocortical projections. Nat. Neurosci. *10*, 1151–1159. https://doi.org/10.1038/nn1960.
69. Morrow, E.M., Yoo, S.-Y., Flavell, S.W., Kim, T.-K., Lin, Y., Hill, R.S., Mukaddes, N.M., Balkhy, S., Gascon, G., Hashmi, A., et al. (2008). Identifying Autism Loci and Genes by Tracing Recent Shared Ancestry. Science *321*, 218–223. https://doi.org/10.1126/science.1157657.
70. Kleefstra, T., Schenck, A., Kramer, J.M., and van Bokhoven, H. (2014). The genetics of cognitive epigenetics. Neuropharmacology *80*, 83–94. https://doi.org/10.1016/j.neuropharm.2013.12.025.
71. Zhang, Q., Huang, Y., Zhang, L., Ding, Y.-Q., and Song, N.-N. (2019). Loss of Satb2 in the Cortex and Hippocampus Leads to Abnormal Behaviors in Mice. Front. Mol. Neurosci. *12*, 33. https://doi.org/10.3389/fnmol.2019.00033.
72. Dent, E.W., Merriam, E.B., and Hu, X. (2011). The dynamic cytoskeleton: backbone of dendritic spine plasticity. Curr. Opin. Neurobiol. *21*, 175–181. https://doi.org/10.1016/j.conb.2010.08.013.
73. Srivastava, A.K., and Schwartz, C.E. (2014). Intellectual disability and autism spectrum disorders: Causal genes and molecular mechanisms. Neurosci. Biobehav. Rev. *46*, 161–174. https://doi.org/10.1016/j.neubiorev.2014.02.015.
74. Giannandrea, M., Bianchi, V., Mignogna, M.L., Sirri, A., Carrabino, S., D'Elia, E., Vecellio, M., Russo, S., Cogliati, F., Larizza, L., et al. (2010). Mutations in the small GTPase gene RAB39B are responsible for X-linked mental retardation associated with autism, epilepsy, and macrocephaly. Am. J. Hum. Genet. *86*, 185–195. https://doi.org/10.1016/j.ajhg.2010.01.011.
75. El-Brolosy, M.A., Kontarakis, Z., Rossi, A., Kuenne, C., Günther, S., Fukuda, N., Kikhi, K., Boezio, G.L.M., Takacs, C.M., Lai, S.-L., et al. (2019). Genetic compensation triggered by mutant mRNA degradation. Nature *568*, 193–197. https://doi.org/10.1038/s41586-019-1064-z.
76. Kozol, R.A., Cukier, H.N., Zou, B., Mayo, V., De Rubeis, S., Cai, G., Griswold, A.J., Whitehead, P.L., Haines, J.L., Gilbert, J.R., et al. (2015). Two knockdown models of the autism genes SYNGAP1 and SHANK3 in zebrafish produce similar behavioral phenotypes associated with embryonic disruptions of brain morphogenesis. Hum. Mol. Genet. *24*, 4006–4023. https://doi.org/10.1093/hmg/ddv138.